

We are IntechOpen, the world's leading publisher of Open Access books Built by scientists, for scientists

5,600

Open access books available

137,000

International authors and editors

170M

Downloads

Our authors are among the

154

Countries delivered to

TOP 1%

most cited scientists

12.2%

Contributors from top 500 universities



WEB OF SCIENCE™

Selection of our books indexed in the Book Citation Index
in Web of Science™ Core Collection (BKCI)

Interested in publishing with us?
Contact book.department@intechopen.com

Numbers displayed above are based on latest data collected.
For more information visit www.intechopen.com



Imaging of Pediatric Benign Bone Tumors

Jignesh Shah and Ankita Chauhan

Abstract

Benign bone tumors in the pediatric population can have varied clinical presentations ranging from asymptomatic to nonspecific pain, swelling, or pathological fracture. A systemic imaging approach should be utilized to evaluate for focal bone abnormalities. Radiologists must be aware of salient imaging features of pediatric benign bone tumors, as it helps to guide clinicians for further management and help decreasing patient anxiety and unnecessary medical intervention.

Keywords: Pediatric benign bone tumors, Osteoid Osteoma, Enchondroma, Non-Ossifying Fibroma

1. Introduction

Primary benign bone tumors are more common than malignancies in children. The patient's age and lesion location are two critical factors when evaluating for a bone tumor. The initial imaging modality to evaluate for a bone tumor is radiography. Radiographs confirm the presence and location of a tumor, assist in the formulation of differential diagnosis, characterize the tumor, and guide in selecting further imaging. Cross-sectional imaging is helpful for tissue characterization and for evaluating the extent of the lesions. The patient's age helps to narrow down the differential diagnosis.

2. Classification

Pediatric benign bone tumors based on the peak age of occurrence:

Child (0–10 years).

Eosinophilic Granuloma.

Simple bone cyst.

Adolescent (10–20 years).

Aneurysmal bone cyst.

Chondroblastoma.

Chondromyxoid fibroma.

Fibrous dysplasia.

Osteochondroma.

Nonossifying fibroma/fibrous cortical defect.

Osteoblastoma.

Periosteal chondroma.

Simple bone cyst.

Adult:

Enchondroma.

Giant cell tumor.

Osteoblastoma.

Brown Tumor (Hyperparathyroidism).

The location of the lesion in the bone can help narrow down the differential diagnosis.

Pediatric benign bone tumors based on location in the long bones:

Epiphysis:

Chondroblastoma.

Giant cell tumor.

Metaphysis:

Aneurysmal bone cyst.

Chondromyxoid fibroma.

Enchondroma.

Nonossifying fibroma/fibrous cortical defect.

Osteochondroma.

Simple bone cyst.

Diaphysis:

Fibrous dysplasia.

Nonossifying fibroma/fibrous cortical defect.

Osteochondroma.

Osteofibrous dysplasia.

Simple bone cyst.

Aneurysmal bone cyst.

Enchondroma.

Some lesions are solitary, and others are multifocal at presentation. The following are the examples of multifocal pediatric benign bone lesions:

Brown tumors (hyperparathyroidism).

Cystic angiomatosis/lymphangiomatosis.

Enchondroma (Ollier disease, Maffucci syndrome).

Fibrous dysplasia (McCune-Albright syndrome).

Infiltrate myofibromatosis.

Langerhans cell histiocytosis.

Nonossifying fibroma (Jaffe-Campanacci Syndrome).

Osteochondroma (Diaphyseal Aclasis).

Chronic recurrent multifocal osteomyelitis (CRMO).

The following features are characteristic for nonaggressive benign bone lesions and help differentiate from aggressive malignant bone lesions:

Well-defined margins with a narrow zone of transition.

Expansion of bone from slow growth.

Smooth periosteal new bone formation.

Absence of an associated soft tissue mass.

Some benign bone tumors are adequately defined by radiographs and do not require any further imaging for diagnosis or treatment. However, most bone tumors require additional imaging; this may be in the form of CT, MRI, scintigraphy, PET scanning, and rarely ultrasound. The choice of imaging for a given tumor depends on the differential diagnostic considerations, possible treatment options, and whether the lesion is aggressive or nonaggressive.

Classification of pediatric bone tumors according to matrix or tissue type:

Cystic lesions: Unicameral (simple) bone cyst, aneurysmal bone cyst.
Osteoid matrix lesions: Enostosis, osteoma, osteoid osteoma, osteoblastoma.
Chondroid matrix: Enchondroma, chondroblastoma, chondromyxoid fibroma, osteochondroma, juxtacortical chondroma.
Fibro-osseous lesions: Nonossifying fibroma, fibrous dysplasia, osteofibrous dysplasia.
Fat containing lesions: Lipoma.
Vascular malformations: Hemangioma.
Giant cell tumors: Giant cell tumor.
Others: Langerhans cell histiocytosis.

3. Primary benign bone tumors by tissue type

Cystic bone lesions:

1. Simple bone cyst:

A simple bone cyst is also called a solitary cyst or unicameral bone cyst (UBC). A simple bone cyst is a common benign nonneoplastic lucent bony lesion mainly seen in childhood and typically asymptomatic. Approximately 85% of unicameral bone cysts occur in children and adolescents [1]. There is 2–3:1 male predominance [2]. During the active phase, the cyst increases in size and remains close to the physis. The latent phase cysts are found farther from the physis and usually do not continue to grow. Cysts may appear to migrate into diaphysis, but actually, it is the growth plate that migrates away from the cyst. The lesions are usually asymptomatic and found incidentally, although the adjacent joint's pain, swelling, and stiffness can also occur. The most frequent complication is a pathologic fracture, and this is usually the cause of presentation. 75% of patients come in with a pathologic fracture [3]. Pathologically, the cysts contain clear serosanguineous fluid surrounded by fibrous membranous lining. The proximal humerus is the most common location (in 50–60% of cases) [4]. The second most common location is the proximal femur.

On radiography, bone cysts are located centrally in the medullary cavity within the metaphysis. Most cysts are less than 3 cm in short-axis diameter but may be much larger in the long axis. The cyst wall is well-defined and sclerotic; the overlying cortex is thinned, and the lesion may be mildly expansile (**Figures 1A, 2A**). Following a fracture, a fragment of bone may be seen dependently within the cyst, called a fallen fragment sign, considered pathognomonic for a simple bone cyst [5] (**Figure 3A**).

Computed Tomography (CT) scan and Magnetic Resonance Imaging (MRI) can help exclude other entities that can potentially mimic a simple bone cyst such as an intraosseous lipoma, fibrous dysplasia, eosinophilic granuloma, giant cell tumor, nonossifying fibroma, or aneurysmal bone cyst. The CT scan helps to delineate the cyst and confirms a fallen fragment. MRI confirms the cystic nature of the lesion. The fluid contents are low signal on T1 and high signal on T2-weighted imaging (**Figure 1B and C**). In contrast, the cyst lining enhances, but the contents do not (**Figures 1D, 2C**). Occasionally, when presenting with intralesional hemorrhage from fracture, fluid–fluid levels may be seen representing internal degraded blood products. The internal hemorrhage may evolve into septations that can be demonstrated on MRI (**Figure 2B**).

On scintigraphy, the unicameral bone cyst appears as a focus of photopenia (cold spot). It may have increased uptake peripherally, and a photopenic center sometimes referred to as a doughnut sign. However, a pathologic fracture would cause an increased radioisotope activity.

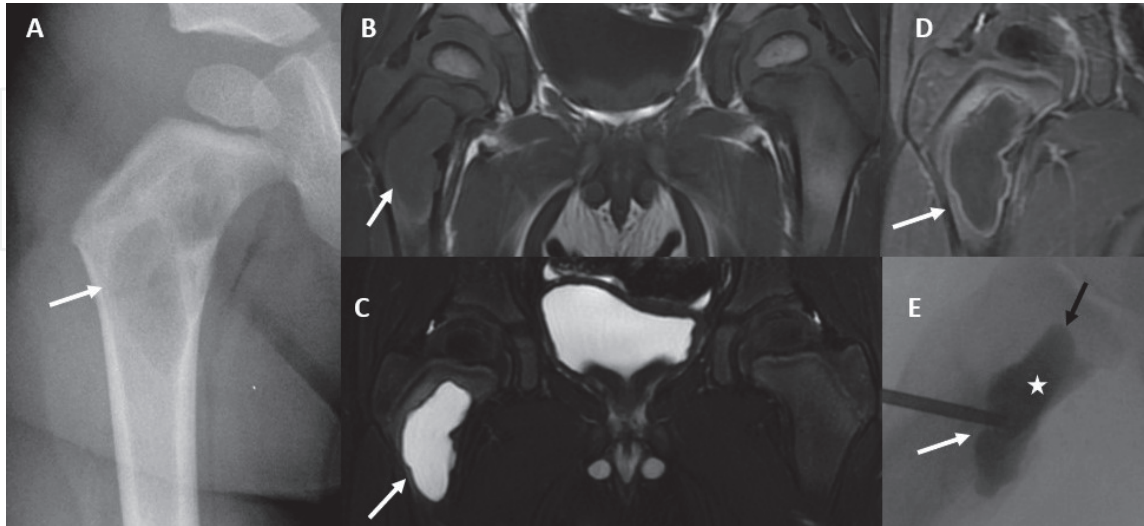


Figure 1.

Simple Bone Cyst: Frontal radiograph of the right femur demonstrates a well-circumscribed, lytic, proximal metadiaphyseal lesion (white arrow) with a narrow zone of transition and represents a simple bone cyst (A). There is no fracture. On the coronal MR sequences (B–D), the simple bone cyst (white arrows) shows an intermediate signal on T1-weighted sequence (B), a homogeneous increased signal on T2-weighted imaging (C), and peripheral rim enhancement on the post-contrast T1-weighted fat-saturated imaging (D). A simple bone cyst is treated by bone grafting. Fluoroscopic spot image of the right femur (E) confirms that the osteolytic lesion is cemented by the bone graft material (white asterisk).

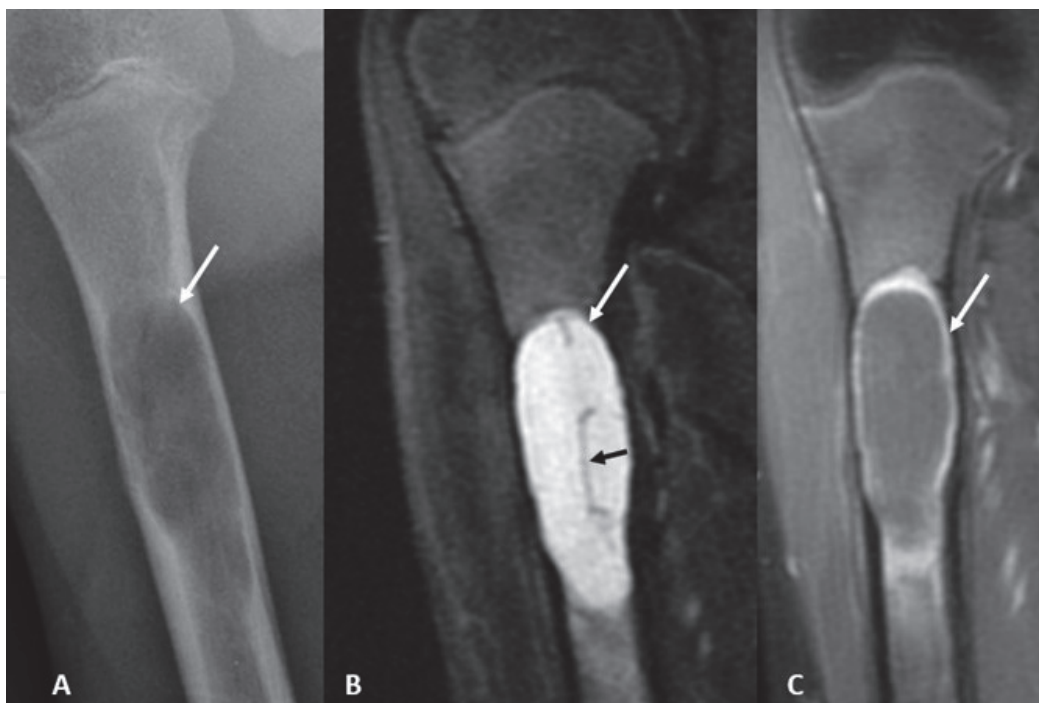


Figure 2.

Simple Bone Cyst: Frontal radiograph of the right humerus (A) demonstrates an expansile circumscribed lytic lesion (white arrow) in the proximal diaphysis with a narrow zone of transition. It has scalloped margins, suggesting chronicity. No cortical breach is demonstrated. Coronal T2-weighted fat-saturated MR image (B) reveals heterogeneous hyperintense signal of the simple bone cyst (white arrow) with a few thin linear T2-hypointensities (septations; black arrow) within. The bone cyst (white arrow) demonstrates peripheral rim enhancement on the post-contrast T1-weighted fat-saturated image (C).

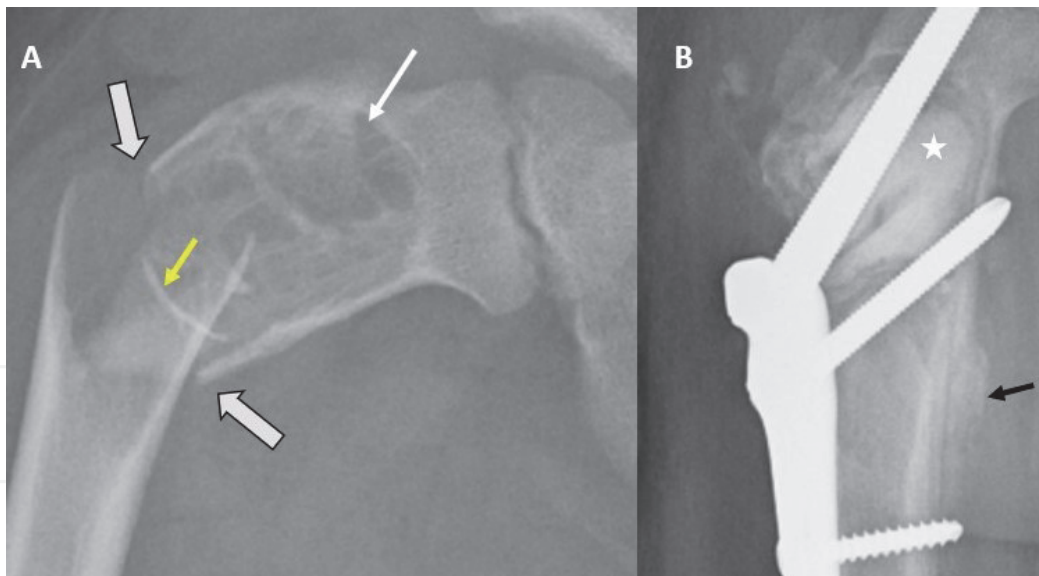


Figure 3. Simple Bone Cyst: Frontal radiograph of the right femur (A) demonstrates a pathological fracture (thick arrows) through a circumscribed expansile lytic proximal meta-diaphyseal lesion (white arrow). It represents a simple bone cyst with the characteristic fallen-fragment sign (yellow arrow). A follow-up post-treatment frontal radiograph of the right femur (B) shows graft material (white asterisk) cementing the bone cyst and a transfixed healing fracture with good periosteal reaction (black arrow).

The larger cysts with or without fracture are usually treated with curettage and bone grafting [6] (**Figures 1E, 3B**). The fractured cyst tends to heal spontaneously. The prognosis is excellent, although 25% of bone cysts recur after curettage [7]. Cyst aspiration with corticosteroid injection or sclerotherapy has also been used for treatment. Intervention is usually not required for an asymptomatic lesion.

2. Aneurysmal bone cyst:

An aneurysmal bone cyst is a benign, radiolucent, expansile, and hemorrhagic lesion of uncertain etiology. Pathologically, the lesion comprises numerous blood-filled nonendothelialized channels separated by connective tissue of bone or osteoid tissue and osteoclastic giant cells. Aneurysmal bone cyst affects 0.14 per 1,00,000 of the population [8]. There may be a slight female predominance. 75–90% of cases occurred before the age of 20 [9]. The patient usually presents with nonspecific pain and swelling, and a minority of patients (approximately 10%) present with pathological fractures. The lesions are most commonly located in the metaphysis of long bones, the craniofacial bones, and the spine; spinal lesions occur in the posterior elements.

The aneurysmal bone cysts are sharply defined on radiographs and appear as expansile osteolytic lesions with thin sclerotic margins, frequently termed a soap bubble lesion [10] (**Figures 4A, 5A**). If the lesion is wider than the affected normal bone, an ABC should be considered. ABCs are typically multiloculated, and the cortex is usually intact but maybe markedly thinned to the point of being invisible, and the periosteal new bone may be present. CT scan demonstrates these findings better and accurately assesses cortical breach and extension to the soft tissues (**Figure 5C**). Additionally, the CT and MRI demonstrate fluid–fluid levels, which are characteristic of the lesion (**Figures 4C, 5B**). Fluid–fluid levels are due to the dependent location of degraded blood products, especially methemoglobin, which has a much shorter T1 relaxation time than hemoglobin. Fluid–fluid levels may be single

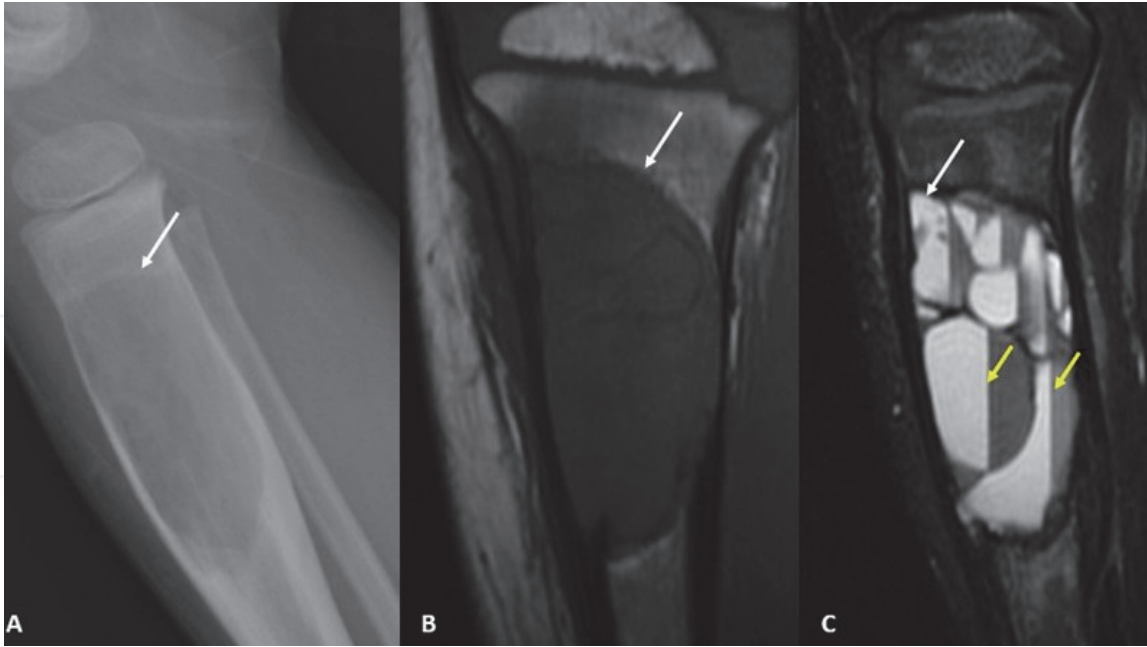


Figure 4.
Aneurysmal Bone Cyst: Lateral radiograph of the left tibia (A) shows a well-circumscribed, expansile, lytic lesion (white arrow) involving the proximal tibial metadiaphysis. It demonstrates internal heterogeneity and has a narrow zone of transition. Coronal T1-weighted image (B) reveals the multiloculated appearance of the lesion (white arrow) and a predominantly intermediate T1 signal. No associated soft tissue swelling is noted. Sagittal fat-saturated T2-weighted image (C) shows multiple fluid-fluid levels within the lesion (yellow arrows), a characteristic imaging feature of an aneurysmal bone cyst.

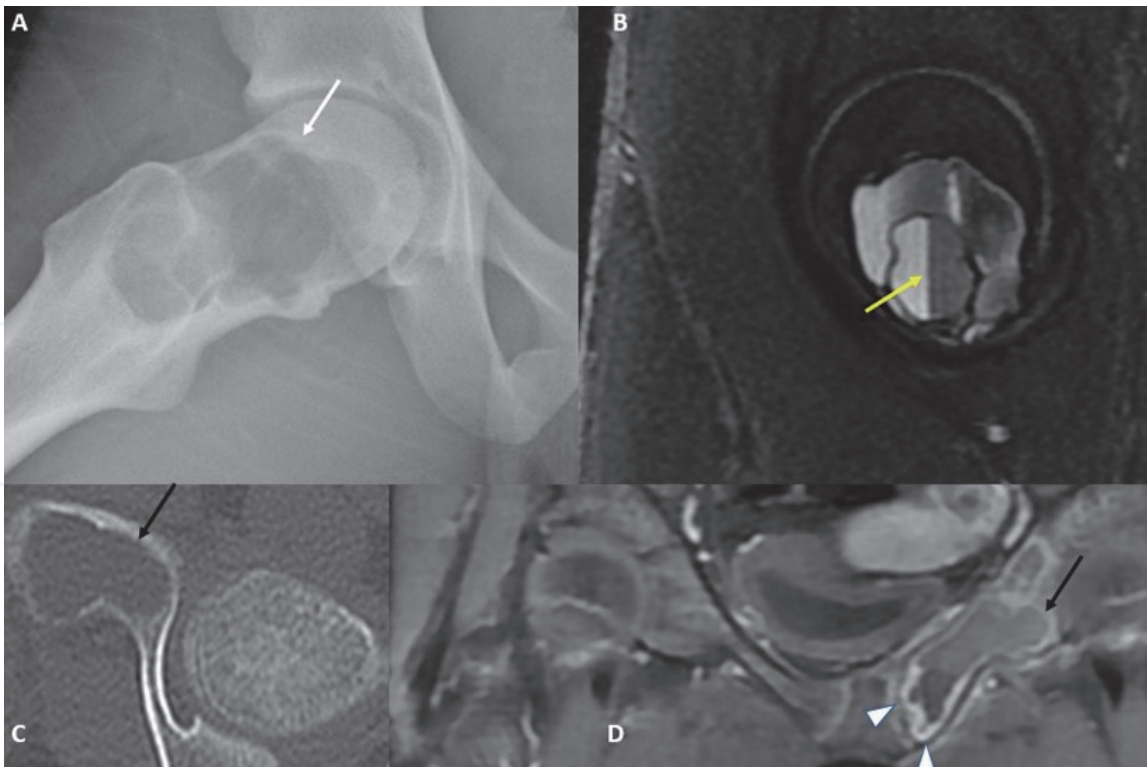


Figure 5.
Aneurysmal Bone Cyst: Lateral radiograph of the pelvis (A) shows an expansile, circumscribed, lytic, proximal femoral metaphyseal lesion (white arrow) with scalloped margins. On axial fat-saturated T2-weighted imaging (B), the lesion shows multiple fluid-fluid levels within (yellow arrow), suggesting an aneurysmal bone cyst. C and D are images of an aneurysmal bone cyst in the left pubic bone in a different patient. The aneurysmal bone cyst appears as a well-circumscribed lytic lesion on CT (C). Coronal T1-weighted fat-saturated post-contrast image (D) depicts heterogeneous and peripheral enhancement of the aneurysmal bone cyst.

or multiple and may be seen as varying horizontal levels within the separate loculations [11]. The signal characteristics of the cyst contents depend on the relative age and concentration of blood components. Abundant hemosiderin may produce areas of low signal. On T1, the cyst is predominantly hypointense (**Figure 4B**). Cyst contents do not enhance, but the septations and wall do (**Figure 5D**).

It may not be possible to differentiate primary and secondary ABCs. Approximately 30% ABCs are secondary [12]. According to one study, the most common reasons for secondary ABC are chondroblastoma and giant cell tumor [13]. Secondary ABC can also be found in other lesions such as osteoblastoma, chondromyxoid fibroma, fibrous dysplasia, and nonossifying fibroma.

Treatment: Most ABCs are treated with curettage and bone grafting. Recurrence rate is approximately 12–30% after initial treatment [14]. Percutaneous treatment with fibrosing agents has also been performed, either in isolation or as a precursor to surgical excision. According to one institution's experience, many ABCs can be treated with polidocanol sclerotherapy [15]. Vascular embolization has also been used. MRI is helpful to identify any solid components which can guide the surgeon for biopsy.

Bone lesions containing osteoid matrix:

1. Enostosis:

Enostosis, also known as the bone island, is a benign focus of compact (cortical) bone located within the cancellous bone (medullary cavity). The bone island is most commonly found incidentally. Pathologically, a bone island is a normal cortical bone containing Haversian canals. There are radiations of cortical bone blending into the normal cancellous bone at the periphery of the lesion. The bone island is likely developmental, a normal cortical bone that fails to resolve during the growth process of endochondral ossification. The bone island is seen in adults far more frequently than children. There is no gender predilection. The bone island is generally a radiographic diagnosis. The bone island is a homogeneously dense lesion on radiography, fading at the periphery and merging into normal marrow. The periphery of the bone island is described as brush-like; may appear somewhat stellate [16] (**Figure 6A**). There is no associated cortical destruction. Polyostotic bone islands concentrated in the metaphyseal region are termed

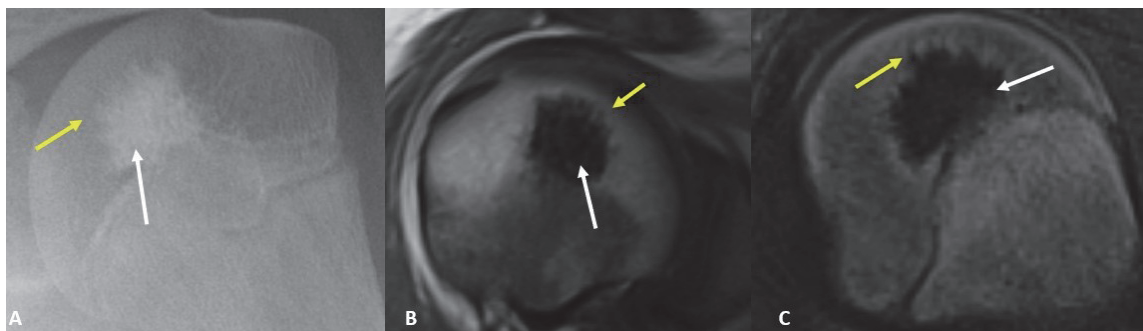


Figure 6.
Enostosis: Frontal radiograph of left humerus (A) shows a circumscribed focal sclerosis (white arrow) in the proximal epiphysis with peripheral brush border extensions into the normal adjacent bone. Axial T1-weighted (B) and T2-weighted fat-saturated (C) images reveal marked hypointense signal of the bone island.

osteopoikilosis. Multiple sclerotic bone lesions can also be seen in patients with tuberous sclerosis complex [17].

On CT scan, enostosis is a sclerotic lesion with peripheral brush border extensions into the normal adjacent bone. Enostosis generally has a mean CT attenuation above 885 Hounsfield units (HU), whereas untreated osteoblastic metastases have mean CT attenuation below 885 HU, according to one study [18]. On MRI, the enostosis demonstrates low signal on all sequences with characteristic peripheral brush border extension into the normal bone (**Figure 6B and C**). There is no postcontrast enhancement. On nuclear medicine scintigraphy, if the lesion size is more than 1 cm, increased radiotracer uptake is related to the osteoblastic activity. SPECT CT has a sensitivity of up to 90% in detecting sclerotic bone metastases [19]. No treatment is required for enostosis.

2. Osteoma:

Osteoma is a benign tumor that demonstrates well-differentiated bone formation without aggressive features. Synonyms of osteoma include surface osteoma, parosteal osteoma, ivory osteoma, Ivory exostosis, and hamartoma of bone. Pathologically, osteoma is a hard white dense cortical bone. Many osteomas demonstrate a mixture of bone types. Osteomas may contain cancellous (trabecular, spongy) regions with a thin trabecular architecture with fatty marrow; woven bone with a fairly mature matrix with prominent collagen fibers; and lamellar (compact regions), which have narrow parallel layers of mature bone matrix. Most commonly, osteomas are found incidentally, with less than 5% of osteomas are symptomatic. The symptoms may be related to the mass effect upon the adjacent soft tissue structures, including proptosis, diplopia, sinusitis, mucocele, abscess as a complication of sinus blockage. Osteoma affects all age groups, including children, although most commonly diagnosed in the fourth and fifth decades of life [20]. The male to female ratio is 2:1. More than 75% of osteomas are seen in paranasal sinuses. The most common paranasal sinus affected is the frontal sinus (80% cases) [21]. Gardner syndrome has a known association with osteoma. Gardner syndrome is an autosomal dominant condition in which the patient may also have multiple cutaneous and subcutaneous lesions (cyst, fibromas), desmoid tumors, and multiple colonic polyps (colonic polyps in Gardner's syndrome have a marked propensity to develop adenocarcinoma).

In radiography and CT scan, the osteoma is seen as a homogeneous bone density lesion due to well-differentiated lamellar bone formation. The borders of osteomas are sharply demarcated (**Figure 7A–D**). There is no periosteal reaction. On MRI, osteomas are seen as low signal intensity on all sequences, without enhancement. Enhanced MRI or CT scan is best to evaluate complications such as mucocele, pneumatocele, or abscess. Treatment is required if intracranial or intraorbital extension, location near frontal sinus ostium, more than 50% of the frontal sinus filled by osteoma or unremitting symptoms [22]. The endoscopic approach for resection is effective in low-grade osteomas. In particular, the open approach, the osteoplastic flap approach, is well tolerated for resection of higher grade osteomas [23].

3. Osteoid Osteoma:

Osteoid osteoma is a benign tumor of osteoblastic origin. The osteoid osteoma is often called “nidus” to distinguish it from surrounding reactive sclerosis from host response. There may be a genetic basis in chromosome band 22q13

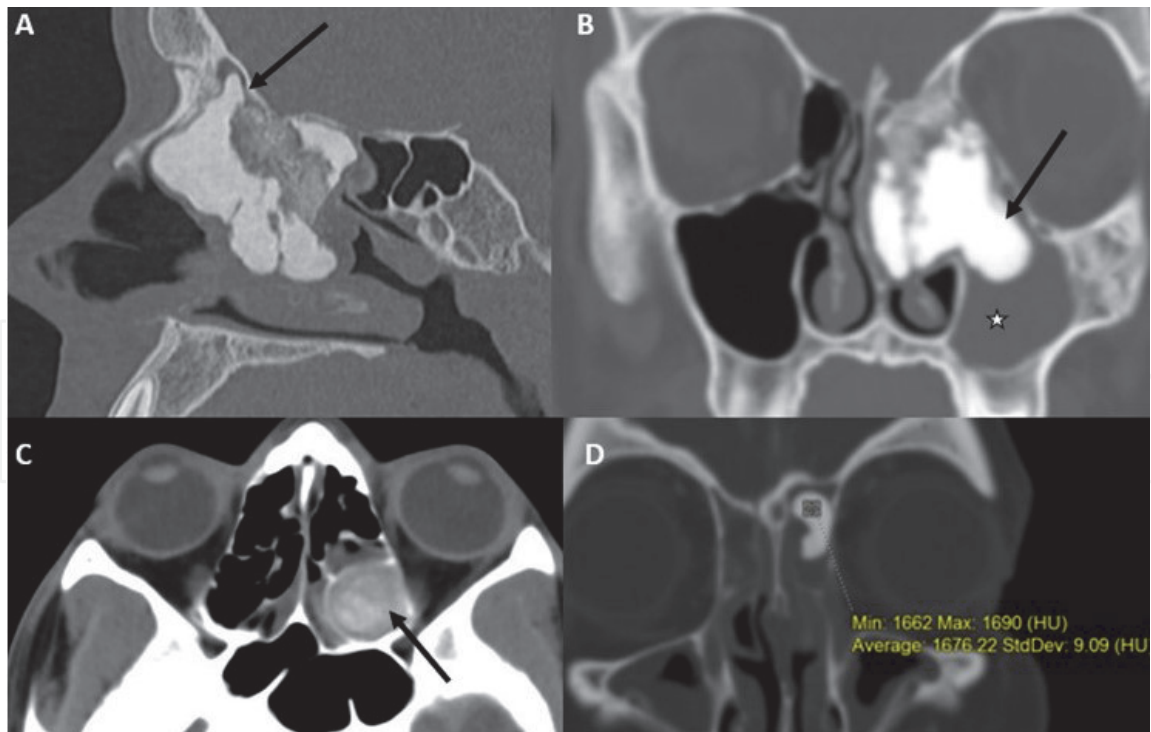


Figure 7.
Osteoma: Sagittal image (bone algorithm, A) and coronal image (bone window, B) of the paranasal sinuses reveal a compact and trabecular sclerotic polypoidal osteoma (black arrows) in the left ethmoid and sphenoid sinuses, extending into the left maxillary sinus with associated occlusion of left osteomeatal unit and left maxillary sinusitis (asterisk). Osteoma can also present as a less dense mass, as depicted by the rounded heterogeneous dense mass in the left posterior ethmoid sinus on the axial CT image (C). Note the high Hounsfield unit of the osteoma (D).

in the patients with osteoid osteoma [24]. The osteoid osteoma contains a central region of vascularized connective tissue that contains osteoblasts and microtrabecular arrays lined by plump appositional osteoblasts. Around the central region, there is a hypervascular sclerotic bone and an abrupt interface between the central lesion and surrounding sclerosis. Osteoid osteoma is relatively common, comprising 5% of all bone tumors and 11% of all benign bone tumors [25]. The most common age range is 10–25 years with a male predilection (Male: female is 3:1) [26]. The classic clinical presentation includes pain, which worsens at night and is relieved by nonsteroidal anti-inflammatory drugs. There is a gradual worsening of the pain over time. Intracapsular lesions may present with signs of synovitis, joint pain, and decreased range of motion. The spinal osteoid osteoma may present with painful nonrotatory scoliosis and concave to the lesion's side [27]. The most common location is cortical diaphyseal, in 65–70% of cases. The most common site involved is femur and tibia, which collectively account for 60% of osteoid osteomas [28]. The nidus is generally less than 2 cm in size.

On radiography, osteoid osteoma appears as an oval lytic lesion located within the dense cortical bone surrounding thickened sclerotic cortical bone (**Figure 8A and B**). CT scan helps diagnose and specify the lesion's location (whether cortical versus subperiosteal or medullary) (**Figure 8C and D**). CT scan is also helpful to guide percutaneous radiofrequency ablation or cryoablation. The nidus is a round lesion on MRI, slightly hyperintense to muscle on T1-weighted images and hyperintense on T2-weighted images. There is avid arterial phase enhancement of the nidus following contrast administration (**Figure 8E**). The surrounding cortical thickening and reaction is low signal intensity on all sequences. In nuclear medicine scintigraphy, the

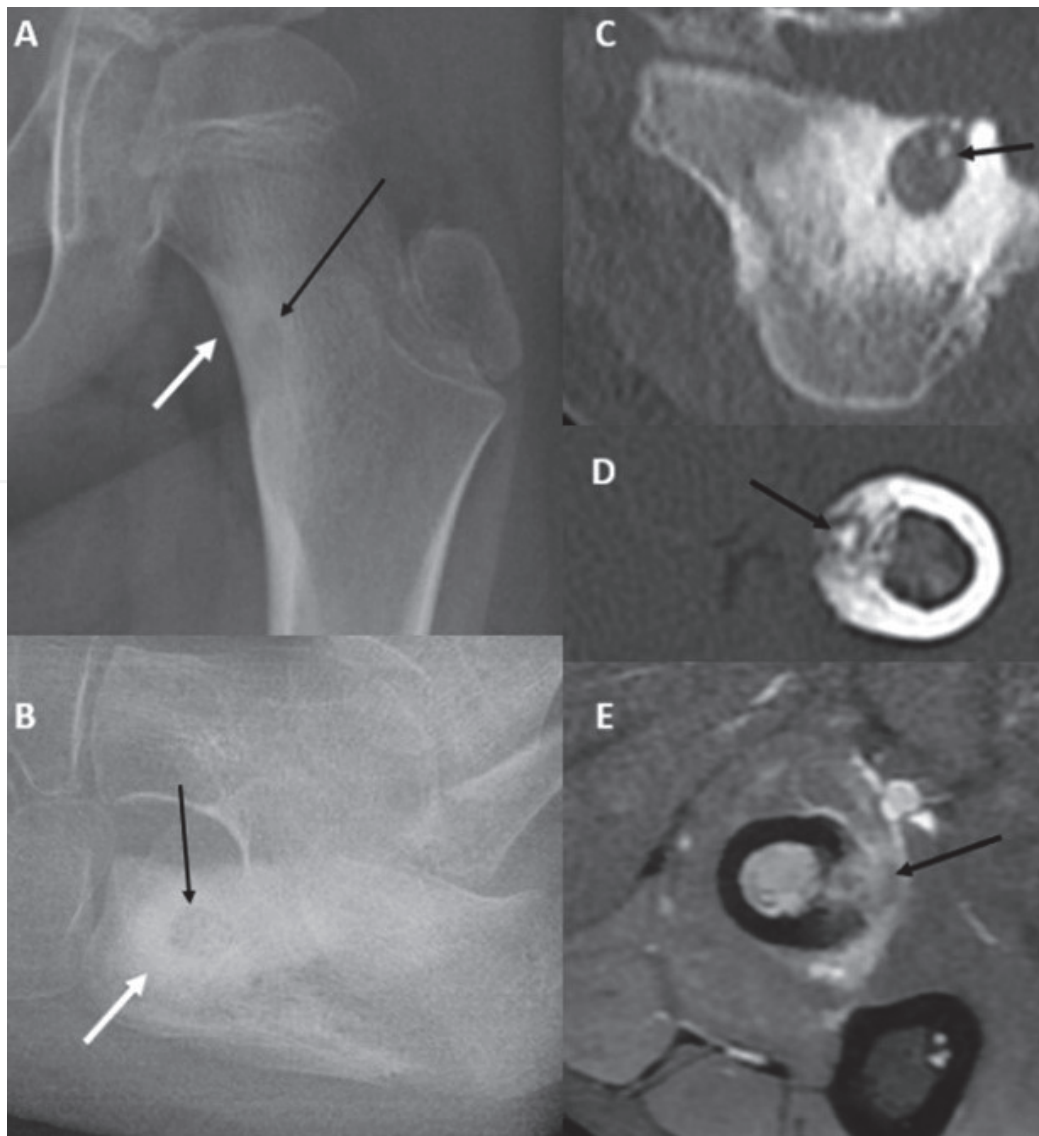


Figure 8.

Osteoid Osteoma: Frontal radiograph of the right femur (A) demonstrates an eccentric lucent area along the medial femoral neck cortex (black arrow) with marginal sclerosis (white arrow). Lateral radiographic view of the calcaneus (B) showing similar lesion with a central lucency surrounded by extensive sclerosis. Axial CT image on the same patient confirms the eccentric location of the lucency that shows an eccentric hyperdense focal speck within, suggesting nidus (C). Osteoid osteoma of the fibula in a different patient appears as a cortical-based lucency with nidus within (black arrow) on axial CT image (D). Axial post-contrast T₁-weighted fat-saturated image (E) of the leg at the same level demonstrates enhancement of nidus (black arrow) and adjacent soft tissue.

osteoid osteoma demonstrates intense round activity at the nidus, surrounded by less intensity of reactive bone, often termed as double density sign [29]. The round focus can help distinguish from a stress reaction, which has more linear activity. CT-guided radiofrequency ablation is most likely used to treat osteoid osteomas with an 85–90% initial success rate [30]. Larger or nonspherical lesions may require a second ablative procedure. The CT-guided ablation requires careful planning of an approach to avoid complications. Other alternatives include MR-guided laser ablation or ultrasound ablation.

4. Osteoblastoma:

Osteoblastoma is a rare benign bone-forming tumor, also known as giant osteoid osteoma. Pathologically, osteoblastoma contains elements of osteoid production in the form of active formation of osteoid and immature bone trabeculae. Aggressive osteoblastoma is characterized by epithelioid

osteoblasts, which are significantly larger than normal osteoblasts. Histologic differentiation between osteblastoma and osteoid osteoma may be difficult. The most commonly affected age group is 1st through third decades, with the second decade being the most common [31]. Male:Female ratio is 2.5:1 [32]. The most common presenting symptom is dull, localized, gradually increasing pain. The patient may present with neurologic symptoms if cord or nerve root compression is reported in approximately 50% of spinal lesions [33]. Approximately 30–40% of osteblastoma occurs in the spine or flat bones [34]. In the spine, posterior elements are most frequently affected (in 94% of cases). The osteblastoma is usually expanded on imaging, maybe bubbly with a thin cortex and variable degrees of mineralized matrix. There may be a sclerotic margin in the majority of the cases. Matrix ossification and thin cortical rim are more apparent on CT scan than x-ray (**Figure 9A–C**).

On MRI, osteblastoma is homogeneous low to intermediate signal on T1-weighted images and heterogeneous on fluid sensitive sequences depending on the degree of matrix ossification (**Figure 9D and E**). The enhancement ranges from mild to intense depending on the amount of matrix ossification. There may be associated extensive peripheral marrow edema and associated soft tissue edema due to the flare phenomenon [35] (**Figure 10A–C**). On nuclear medicine scintigraphy, osteblastoma demonstrates intense focal

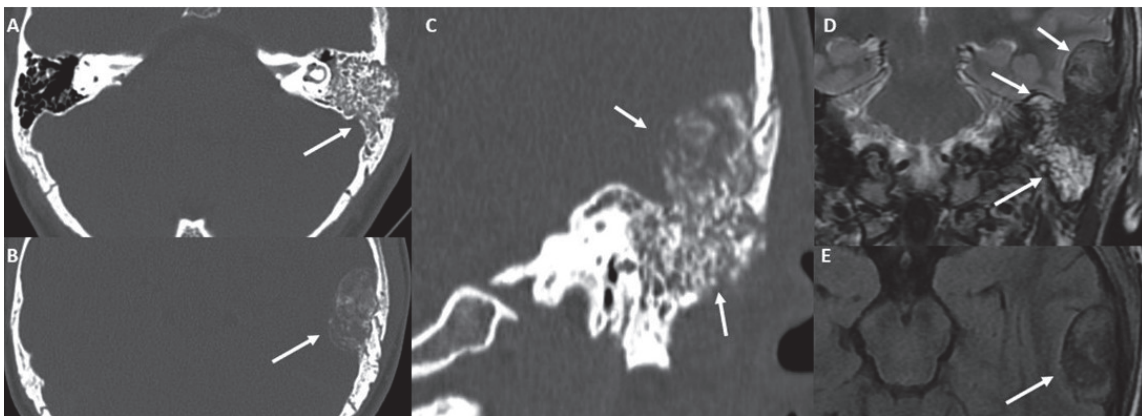


Figure 9. Osteblastoma: CT Head axial (A, B) and coronal (C) images in the bone window reveal a circumscribed, expansile, heterogeneous mixed lytic and sclerotic lesion (white arrows) involving the mastoid part of the left temporal bone and has an extradural intracranial component superiorly. Coronal T2-weighted image (D) of the brain at the level of mass (white arrows) reveals heterogenous increased T2 signal of the well-circumscribed mass. Osteblastoma (white arrow) shows an iso-to-hypointense T1 signal (E).

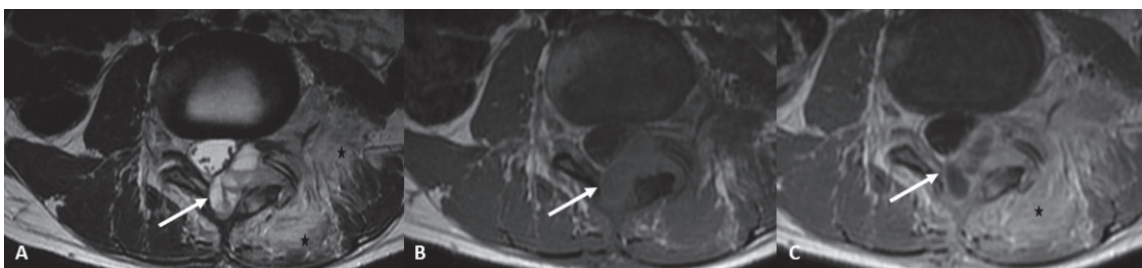


Figure 10. Osteblastoma: Axial MR images of the lumbar spine shows an expansile mass lesion involving the left lamina and pedicle, encroaching in the spinal canal. It demonstrates heterogeneous hyperintense T2 signal (white arrow) with subtle fluid-fluid levels (A). The lesion shows an intermediate T1 signal (B) and shows heterogeneous enhancement as depicted in the T1-weighted post-contrast (C). The left posterior paraspinal muscles demonstrate hyperintense T2 signal and post-contrast enhancement (black asterisks).

uptake. Surgical excision, in particular, marginal excision (curettage), is most recommended if wide resection would result in functional impairment. Incomplete excision may result in recurrence (14–24% reported in different series) [36, 37]. Other treatment options include percutaneous thermal ablation. Sporadic cases of osteblastoma degenerating to osteosarcoma have been reported [38].

Cartilage forming tumors:

1. Enchondroma: Enchondroma is a benign tumor of hyaline cartilage originating in the medullary bone. Enchondromas arise from growth plate cartilage rests and/or chondrocytes that subsequently proliferate and slowly enlarge and are composed of mature hyaline cartilage. The most common location of enchondroma is the medullary cavity of tubular bones. Enchondroma accounts for 12–24% of all benign bone tumors and 3–10% of all bone tumors [39, 40]. Approximately 35% of enchondromas occur in hands [40]. In long bones, the proximal humerus is the most common location. Enchondromas are usually detected incidentally on x-ray or MRI. The majority of enchondromas are detected in the third through fifth decades of life [41]. There is no gender predilection. Enchondroma is the most common tumor of the phalanges of the hand. The classic radiographic appearance of enchondroma in the long bones is a metaphyseal lesion with ring and arc type of chondroid mineralization without endosteal scalloping, cortical destruction, or soft tissue mass (**Figure 11A and B**). In phalanges, the enchondroma demonstrates an expansile lucent lesion with cortical thinning (**Figure 11D and E**). The phalangeal enchondroma may present with pathologic fracture. On MRI, the enchondroma demonstrates low to intermediate signal intensity on T1-weighted images and lobulated high signal on fluid sensitive sequences. Dynamic contrast-enhanced MRI may improve chances of differentiating enchondroma from low-grade chondrosarcoma [42]. Treatment is usually not required for small incidental lesions. For large symptomatic lesions, marginal and/or wide resection should be considered. Sarcoma follow-up surveillance is required if histologic findings showed low-grade chondrosarcoma.

Ollier disease is a nonhereditary, sporadic skeletal disorder characterized by multiple enchondromas principally located in the metaphyseal regions. If there are associated soft tissue hemangiomas, the syndrome is termed Maffucci syndrome [43]. In Ollier disease, the enchondromas demonstrate vertical streaks of lucencies in the columnar configuration, in metaphyses of long bones, extending to the epiphysis [43] (**Figure 12B and C**). The phalangeal lesions are typically expansile with sharply defined scalloped margins (**Figure 12A**). There is an approximately 25–30% risk of chondrosarcoma in the setting of Ollier disease [44]. Corrective surgery is required if there are complications such as growth impairment, deformity such as leg length discrepancy.

2. Chondroblastoma: Chondroblastoma is a benign cartilage tumor arising in the epiphysis of skeletally immature individuals. More than 75% of chondroblastomas occur in long bones [45]. The most common location is epiphysis, with possible extension to metaphysis. Chondroblastoma may have a genetic basis in structural anomalies involving chromosomes 5 and 8 [46]. Macroscopically, there are nodules of relatively mature cartilage surrounded by highly cellular tissue. Giant cells are usually present in the tumor. The most

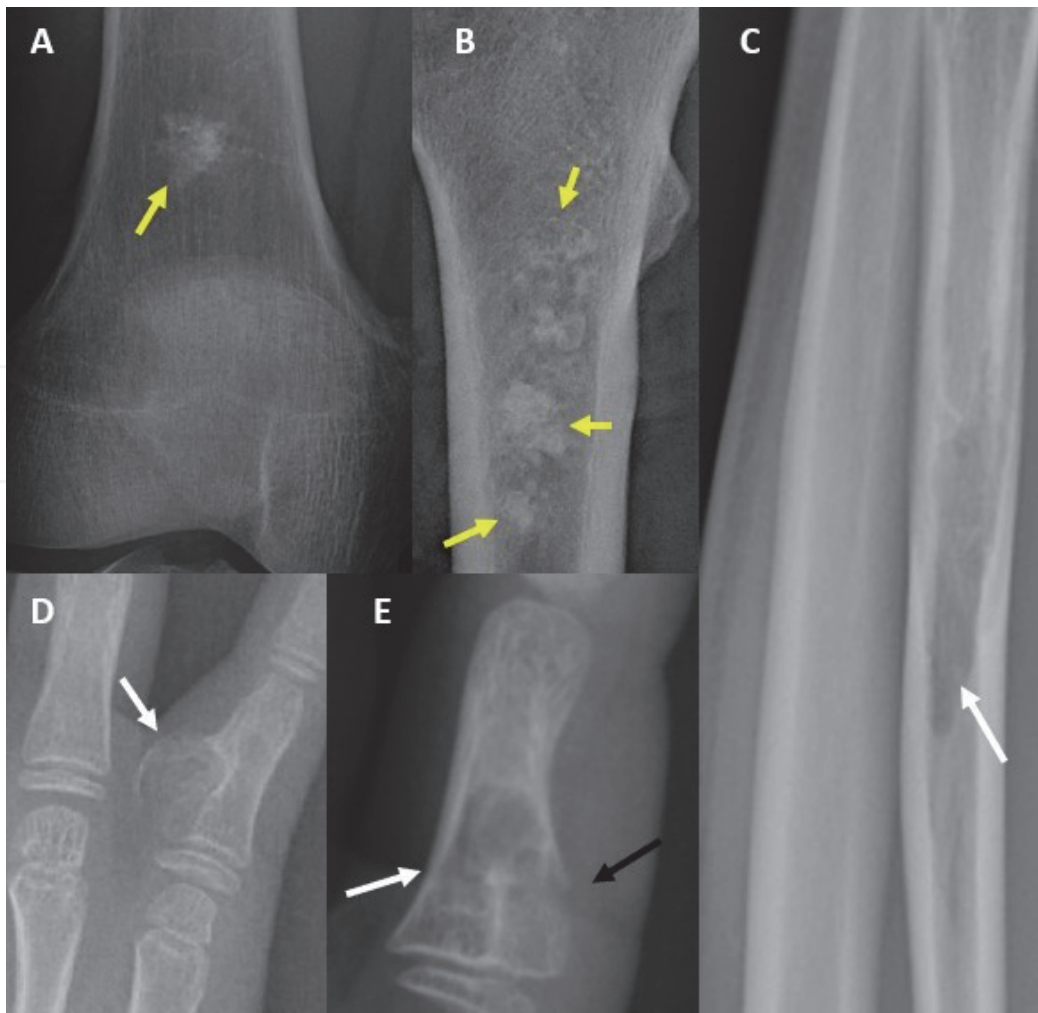


Figure 11.
Enchondroma: Frontal radiograph of the distal femur (A) and proximal femur (B) in two different patients reveal the characteristic rings and arcs pattern of chondroid mineralization (yellow arrows). The lateral radiograph of the forearm (C) shows an expansile lytic lesion (white arrow) in the mid-diaphysis of radius. It demonstrates a narrow zone of transition without any periosteal reaction or associated soft tissue swelling. A frontal radiographic view of the proximal phalanx of the little finger (D) shows a well-defined eccentric osteolytic lesion (white arrow). The frontal radiograph of the index finger (E) shows an expansile well-circumscribed osteolytic lesion (white arrow) with a chondroid matrix. The black arrow points to a cortical breach concerning a pathological fracture.

common presenting symptom is mild localized pain, which refers to joint. The most common age range affected is 10–25 years old. Males are more frequently affected than females (nearly 2:1). Chondroblastoma comprises less than 1% of all bone tumors and approximately 9% of benign bone tumors [47]. The chondroblastoma is a geographic lytic lesion with sclerotic margins in most lesions on radiography and CT scan. The lesion may contain chondroid matrix calcifications. The lesions are eccentrically located within the epiphysis with extension into metadiaphysis as they enlarge. There may be an associated cortical expansion or thinning (**Figure 13A–C**). On MRI, the lesions are typically low signal on T1 and inhomogeneously high signal on fluid sensitive sequences. The inhomogeneity is related to the chondroid matrix, calcification, and fluid within the lesion [48] (**Figure 13D–F**). Curettage and bone grafting is the surgical treatment of choice. Radiofrequency ablation may be considered in small lesions.

3. Chondromyxoid fibroma: Chondromyxoid fibroma is a benign lobulated cartilaginous tumor. Approximately 60% of chondromyxoid fibromas occur in long bones, with the proximal tibia being the single most frequent site. Genetic basis has been described in the literature in the form of clonal abnormalities of

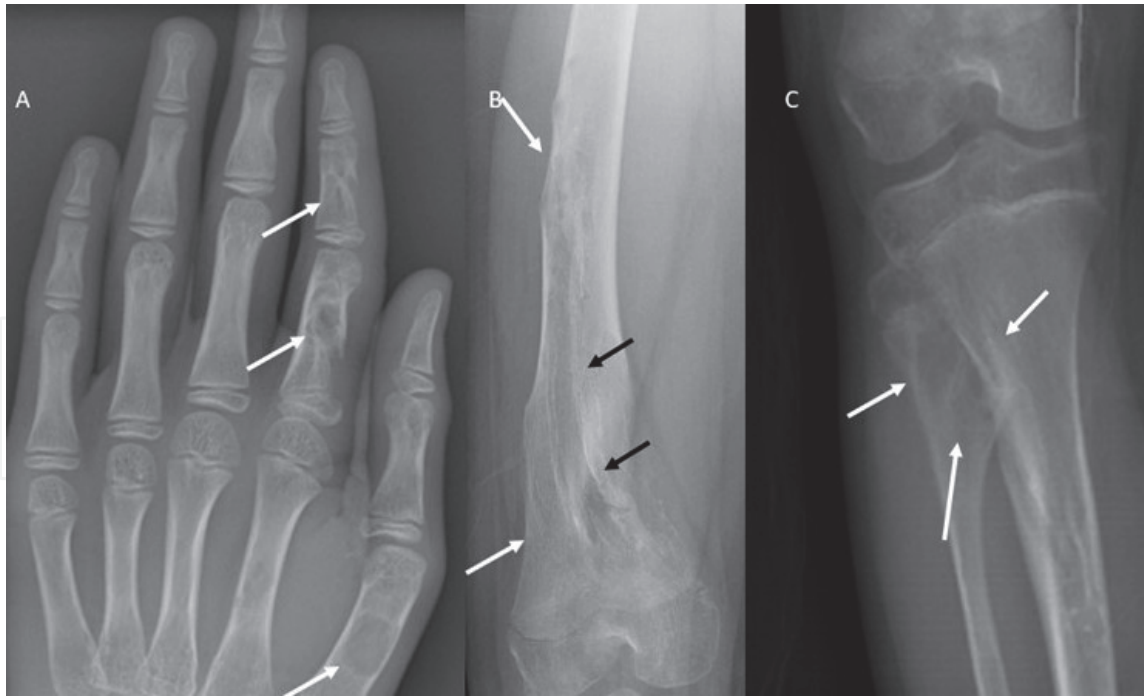


Figure 12.

Ollier's disease: Frontal radiograph of the left hand (A) demonstrates multiple circumscribed lucent areas (white arrows) in hand with a sharp zone of transition. Frontal radiograph of the right femur (B) shows vertical streaks of lucencies (black arrows) extending from diaphysis towards epiphysis. Frontal radiograph of the right tibia and fibula (C) reveals an expansile enchondroma in the proximal fibular metaphysis (white arrows) and a not that much expansile enchondroma in the tibial metadiaphysis.

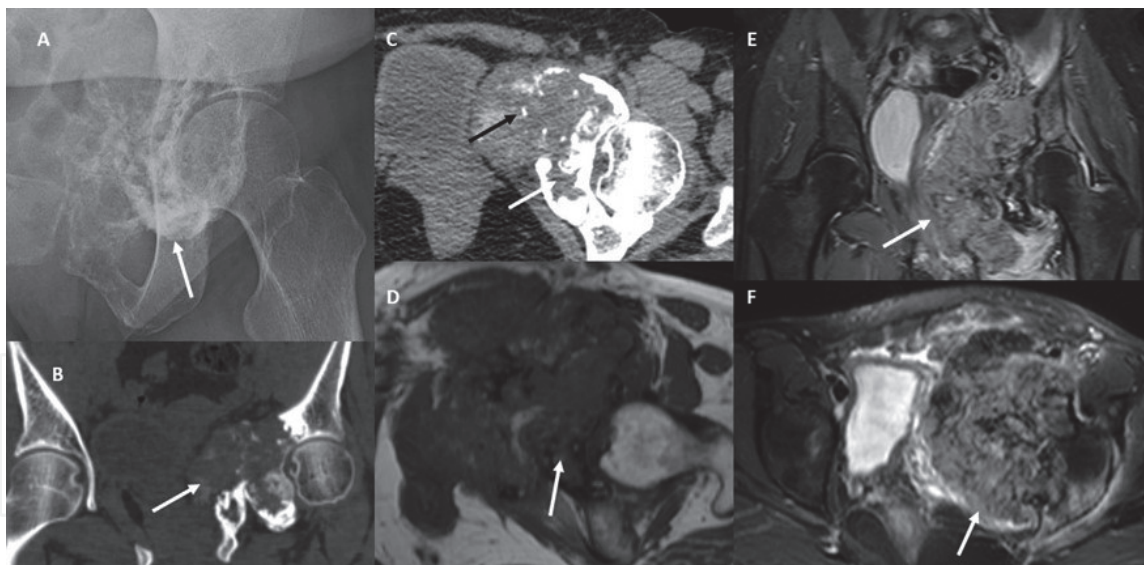


Figure 13.

Chondroblastoma: Frontal radiographic view of the left pelvis (A) shows a calcified mass of the left ischium and pubic bones. Coronal bone window (B) and axial soft tissue window (C) images demonstrate an expansile osteolytic lesion (white arrows) with a well-defined lobulated margin and chondroid matrix (black arrow). Chondroblastoma demonstrates a hypointense T1 signal (white arrow; D) with a peripheral sclerotic rim. Coronal (E) and axial (F) T2-weighted fat-saturated images reveal heterogeneous hyperintense T2 signal of the mass (white arrows) with extensive peritumoral edema.

chromosome 6 and pronounced expression of type II collagen, which is unique compared with other cartilaginous lesions. Microscopically, the lesion is lobular with stellate cells in the myxoid background. The most common presenting symptom is mild chronic pain. The mean age of presentation is 23 years, with 50 percent of patients are in the second decade at presentation. There is slight medial predominance. On radiography and CT, the lesions are

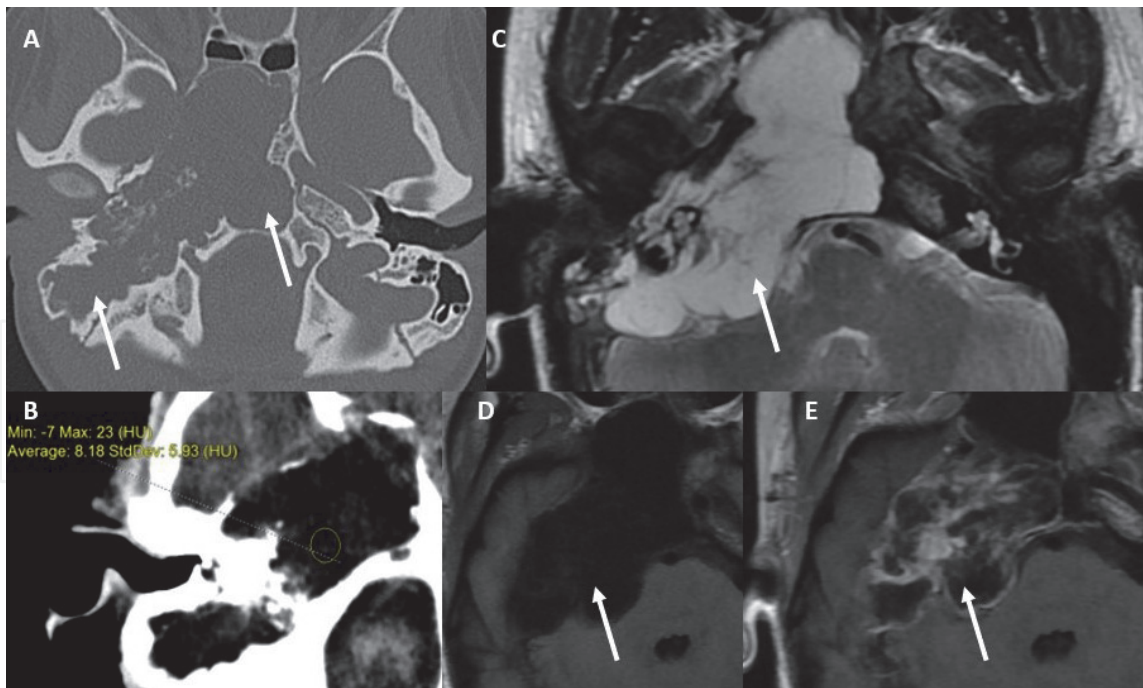


Figure 14. Chondromyxoid fibroma: Bone window (A) and soft tissue window (B) axial CT head images show a well-defined lobulated lytic lesion (white arrows) involving the mastoid and petrous parts of the right temporal bone and clivus. A note is made of the low attenuation value of the CMF lesion and absent calcifications. On the T2-weighted image (C), the CMF lesion demonstrates a peripheral hypointense sclerotic rim with an intrinsic high signal (white arrow). It shows a hypointense T1 signal (D) and shows thick peripheral enhancement (E). MR features to support the diagnosis of the chondromyxoid fibroma (CMF).

geographic with sclerotic margins. The lesions typically occur in metaphysis or diaphysis, which are oriented along the longitudinal axis of the bone.

Approximately 60% of lesions are eccentric, with evidence of lobulation and thinning of the cortex (Figure 14A and B). Pseudotrabeculations within the lesion give the appearance of septations [49]. There is an absence of periosteal reaction without pathologic fracture. On MRI, the lesion is typically isointense to skeletal muscle on T1-weighted images, and on fluid sensitive sequences, the lesion is centrally hyperintense with a peripheral band of intermediate signal. There is a peripheral nodular enhancement or diffuse postcontrast enhancement [50] (Figure 14C–E). The lesions are typically treated with marginal excision with curettage and bone grafting. The recurrence rate is approximately 3–22% [51].

- 4. Osteochondroma:** Osteochondroma is cartilage capped exostosis with continuous cortex and marrow extending from the underlying bone. Osteochondroma most commonly arises from metaphysis or metaphyseal equivalents. Approximately 95% of them are located in extremities; the femur is most commonly affected [52]. Microscopically, the inner layer is composed of normal bone; the middle layer is composed of cartilage cap with superficial clusters of chondrocytes, and the outer layer is composed of perichondrium, which is continuous with the periosteum of the underlying bone. The most common presenting symptom is a chronically present hard swelling. It may present as mechanical pain from trauma or impingement. Vascular complications include pseudoaneurysm formation and arterial or venous stenosis/thrombosis. Increasing pain and/or mass enlargement following skeletal maturation suggest degeneration to chondrosarcoma [53]. Osteochondromas could be sessile or pedunculated. On radiography and CT scan, the pedunculated osteochondroma

demonstrates a narrow stalk with cauliflower exostosis (**Figure 15D**), and the sessile osteochondroma is broad-based (**Figure 15A and C**). If near the joint, osteochondroma tends to project away from the joint line, growing along the forces generated by the location of the tendons and ligaments. The pelvic osteochondromas could become very large before discovery. Rib lesions may present with pneumothorax. Endochondral calcification may be seen within the cartilage cap and medullary bone as the rings and arcs, punctate or flocculent calcification. The overlying cartilage cap is generally thinned, not evaluated by radiograph. Degeneration of the lesion to chondrosarcoma is suggested by osseous destruction, change in calcifications, or enlargement of the cartilage cap as evidenced by distortion of the fat planes. On MRI, the cortex of the lesion is contiguous with the underlying bone. The overlying hyaline cartilage cap has a lobulated high signal on fluid-sensitive sequences covered by thin perichondrium and demonstrates a low signal on T1 and T2 sequences [54] (**Figure 15E and F**). Surgical resection of the osteochondroma is recommended when the cartilage cap thickness is greater than 1 cm. In one study, the use of 2 cm as a cutoff for distinguishing benign osteochondromas from secondary chondrosarcomas provided sensitivities, specificities, positive predictive values, and negative predictive values of 100%, 98%, 96%, and 100%, respectively, for MR imaging and 100%, 95%, 93%, and 100%, respectively, for CT [54]. Treatment is mostly watchful waiting. Resection of the osteochondroma is recommended when there are mechanical complications such as bursa formation, nerve irritation, or impingement. Resection of the entire perichondrium is required to avoid recurrence. Chondrosarcoma is typically treated by wide surgical resection.

Multiple hereditary exostoses, also known as diaphyseal aclasis, is an autosomal dominant condition in which there are multiple sessile and pedunculated osteochondromas. Approximately 90% of patients have a positive family history of this condition [55]. There is a symmetric widening of the metaphysis with the normal underlying bone. Sessile osteochondromas

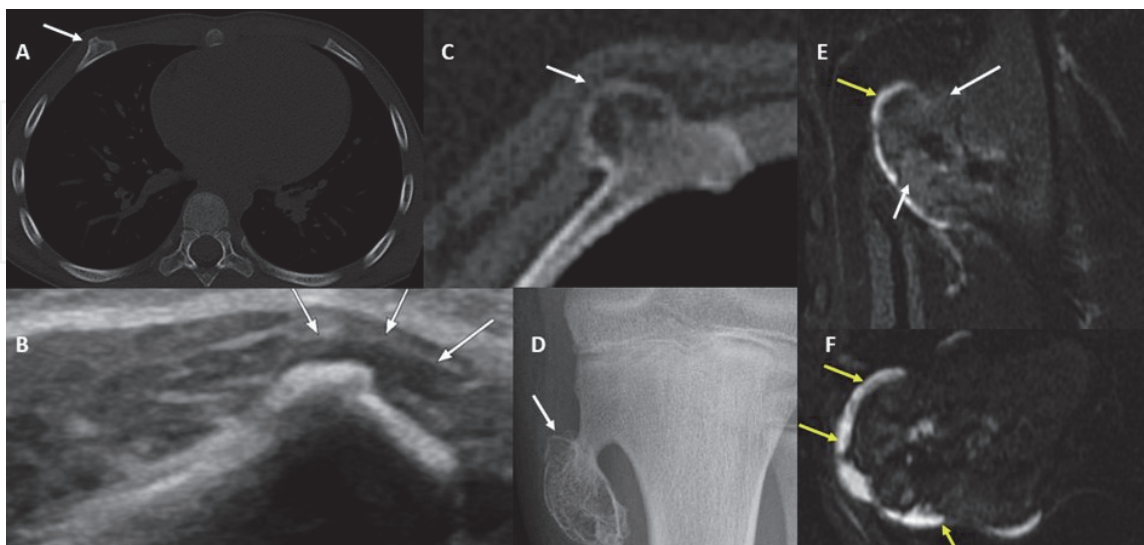


Figure 15.

Osteochondroma: Axial CT bone algorithm image (A) of the mid thorax shows a focal bulge in the anterior right rib (white arrow) with cortical continuity, a finding also appreciated on the longitudinal grayscale ultrasound image (B). It represents a sessile osteochondroma, another example of which is C (white arrow). Frontal radiograph of the left tibia (D) reveals a pedunculated osteochondroma (white arrow) noted in the metaphyseal region, with the cortex of the parent bone (tibia in this case) contiguous with that of the lesion, and the lesion is directed away from the joint. The T2-weighted fat-saturated coronal (E) and axial (F) images reveal the T2 hyperintense cartilage cap (yellow arrows) of that osteochondral lesion (white arrows).

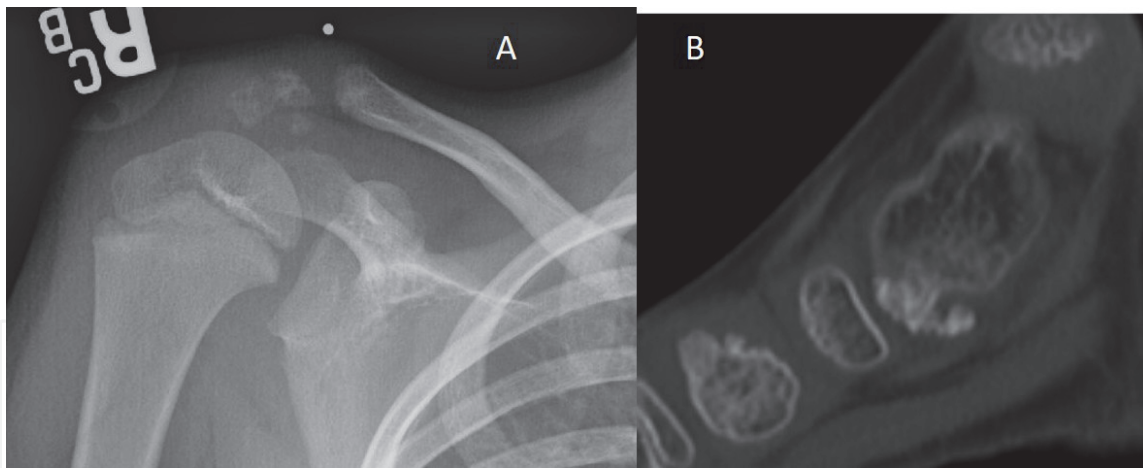


Figure 16.
Trevor disease: Frontal radiograph of the right shoulder demonstrates an osteochondroma arising from right proximal humeral epiphysis, suggesting Trevor Disease (A). Sagittal bone window image of ankle demonstrates an osteochondroma arising from Talus (B).

are more common than pedunculated osteochondromas. There is an approximately 3–5% incidence of degeneration to chondrosarcoma [56]. Radiography is the 1st line modality to evaluate for this condition. MRI can be performed to evaluate the thickness of the cartilage cap and evaluate for complications from the mass effect. If the lesion is superficial, ultrasound can also be used to evaluate for thickness and irregularity of the cartilage cap. Surgical resection is performed if there are complications from mass effect or evidence of degeneration to chondrosarcoma.

Trevor disease, also known as dysplasia epiphysealis hemimelica, is an extremely rare, nonhereditary disease in which the osteochondromas arise from the epiphysis. It affects approximately one in 1 million population [57]. Only one epiphysis is involved in the localized type, although multiple epiphyses are affected involving the entire extremity in generalized type. There is the presence of an exostosis arising from the epiphysis on radiography and CT scan (**Figure 16A** and **B**). Surgical excision of mass is usually performed to preserve the joint.

5. Juxtacortical chondroma: Juxtacortical chondroma is a chondroid tumor arising in the periosteal layer of tubular bones. It is a rare benign tumor comprising less than 2% of chondromas [58]. The most common age range affected is second through fourth decades. Although, it may occur in children. Juxtacortical chondroma is a surface lesion arising from the metaphysis of the tubular bone-producing chondroid matrix. The lesion is located in the proximal humerus and femur in 70% of cases. On radiography, there is saucerization of the cortex with sclerotic margins and matrix calcification (in 75% of cases) (**Figure 17A**). There may be associated soft tissue mass. On MRI, the lesion is lobulated with iso to hypointense T1 signal and hyperintense T2 signal with heterogeneous predominantly peripheral enhancement (**Figure 17B–E**). The tumor demonstrates slow local progression. Wide surgical excision is the most appropriate treatment for lesions greater than 3 cm in size [59].

Fibro-osseous lesions:

1. Fibrous cortical defect: Fibrous cortical defect is the most common benign bone lesion [60]. The most common location is usually metaphysis or

metadiaphysis junction of the femur or tibia. On radiographs, the fibrous cortical defects are eccentric cortically based lucent lesions with mineralized rim (**Figure 18A and B**). There is no involvement of the underlying medullary cavity. There is no periosteal reaction. The fibrous cortical defects are typically hypointense on T1 weighted images and hyperintense on T2-weighted images (**Figure 18C and D**). The signal intensity depends on the stage of healing. Fibrous cortical defects are typically seen incidentally on radiographs. These are no-touch lesions (no treatment is required). Benign fibro-osseous lesions may be metabolically active on FDG PET CT exam and should not be confused with metastases [61].

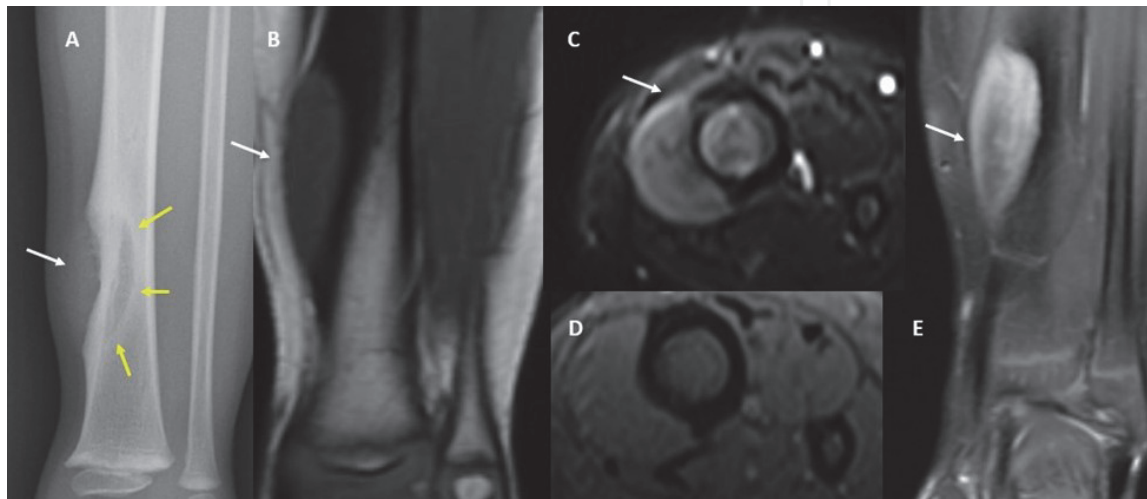


Figure 17.

Juxtacortical chondroma: Frontal radiograph of the left tibia and fibula (A) demonstrates a well-defined distal tibial metadiaphyseal lucent lesion (white arrow) with underlying cortical saucerization or scalloping (yellow arrows) and subjacent cortical sclerosis. It demonstrates a hypointense T1 signal (B) and an increased T2 signal (C). T1-weighted fat-saturated pre (D) and postcontrast (E) images demonstrate peripheral enhancement of the chondroma lesion (white arrow).

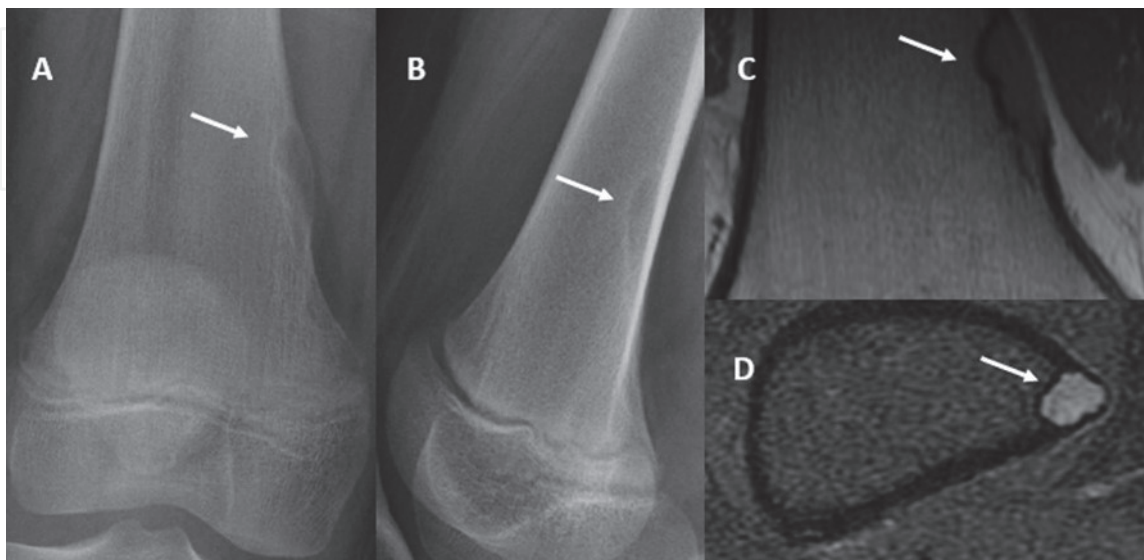


Figure 18.

Fibrous cortical defect: Frontal (A) and lateral (B) radiographs of distal femur demonstrate eccentric lucent intracortical defect (white arrows) outlined by a rim of sclerosis. Note that there is no involvement of the underlying medullary cavity, and there is no periosteal reaction. The lesion (white arrows) demonstrates a hypointense T1 signal (C) and increased T2 signal with a peripheral hypointense sclerotic rim (D).

2. Nonossifying fibroma: Nonossifying fibroma is a benign fibrous lesion composed of spindle cells in a collagenous matrix. Nonossifying fibroma is generally greater than 3 cm in greatest dimension (as opposed to a fibrous cortical defect less than 3 cm in diameter) [62]. Nonossifying fibroma typically originates in the metaphysis and is cortically based, most commonly found around the knee and distal tibia. It can be multifocal in 8% of cases. Multifocal nonossifying fibromas may be associated with neurofibromatosis (Jaffe-Campanacci syndrome). Nonossifying fibroma is usually asymptomatic; however, it could present with pathological fracture. It is typically seen in the first and second decade of life.

Radiographic and CT appearance depends on the morphologic age of the lesion. Initially, the lesion appears as a lytic, geographic area with a thin sclerotic margin (**Figure 19A and B**). During early filling phases, it has a thicker sclerotic margin forming peripheral bone. During late stages, the lesion may be entirely sclerotic with usual remodeling to normal bone type appearance. On MRI, the lesion is hypointense to skeletal muscle on T1 and heterogeneous on fluid sensitive sequences with low signal areas and hyperintense areas (**Figure 19C and D**). The regions of low signal areas are fibrous elements and hemosiderin. There is peripheral and septal enhancement following contrast administration. No cortical destruction or soft tissue mass lesion is demonstrated. No treatment is required in a vast majority of cases. If there is a risk for pathologic fracture due to the size of the lesion, curettage and bone grafting can be performed. Syndromic form of multiple nonossifying fibromas has a higher rate of recurrence after surgical removal [63].

3. Fibrous Dysplasia: Fibrous dysplasia (FD) is a developmental disorder characterized by the replacement of normal bone by immature bone and cartilaginous tissue. Most cases are sporadic and are related to a mutation in the GNAS1 gene. GNAS gene codes for the stimulatory alpha subunit of guanine nucleotide-binding protein, and its mutation result in persistent adenylyl cyclase activation leading to osteoblastic proliferation. FD comprises

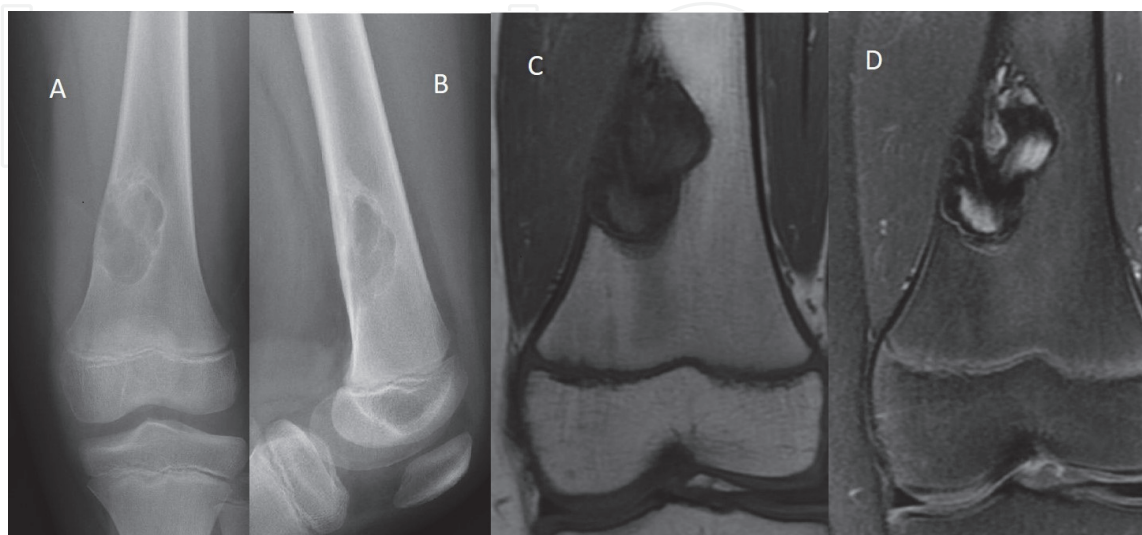


Figure 19. *Non-Ossifying Fibroma: Frontal and lateral radiographs of femur demonstrate an eccentric cortically based radiolucent lesion with sclerotic margin in distal meta-diaphysis (A, B). On MRI of the same patient, the lesion demonstrates predominantly hypointense signal on T1 and heterogenous signal on STIR due to fibrous elements and hemosiderin (C, D).*

about 5–7% of all cases of benign tumors [64]. It can involve any bone and any part of the bone.

Four clinical presentations of FD have been described [65]:

1. Monostotic FD (70–80% of all FD): Single bone is involved (**Figure 20**) with craniofacial involvement in 10–27% of cases. It generally manifests at 10–30 years of age. FD lesions do not demonstrate an increase in size after puberty.
2. Polyostotic FD (20–25%): Multiple bones are affected (**Figure 21**). Craniofacial involvement is seen in 40–100% of cases. It usually manifests before age 10. Polyostotic FD lesions, in some cases, increase in size even after puberty.
3. McCune-Albright syndrome (3%): It is characterized by café-au-lait skin macules, polyostotic fibrous dysplasia, and endocrine hyperfunction disorders (precocious puberty, pituitary adenomas secreting growth hormone, hyperthyroidism, and autonomous adrenal hyperplasia). Increased growth and recurrence of the FD lesions are seen [66]. Some examples include the classic “Shepherd’s crook” deformity of the femur, coxa vara, and scoliosis resulting from spinal FD.
4. Mazabraud syndrome: It is characterized by the coexistence of polyostotic fibrous dysplasia lesion and intramuscular myxomas.

Generally, FD lesions are lytic and well-defined but can look like almost anything and are not associated with soft tissue swelling. The radiographical features of FD can vary from ground-glass appearance, purely cystic (completely lucent) lesions, mixed cystic and sclerotic lesions, to sclerotic lesions. They may demonstrate a geographic (circumscribed) pattern with or without a sclerotic border or appear as expanded lesions with or without associated endosteal scalloping. CT accurately delineates margins of the FD lesions and helps in detecting subtle fractures [67]. FD lesions demonstrate different CT patterns depending upon the patient’s age, varying from homogeneous dense lesions in the pre-pubertal life to a

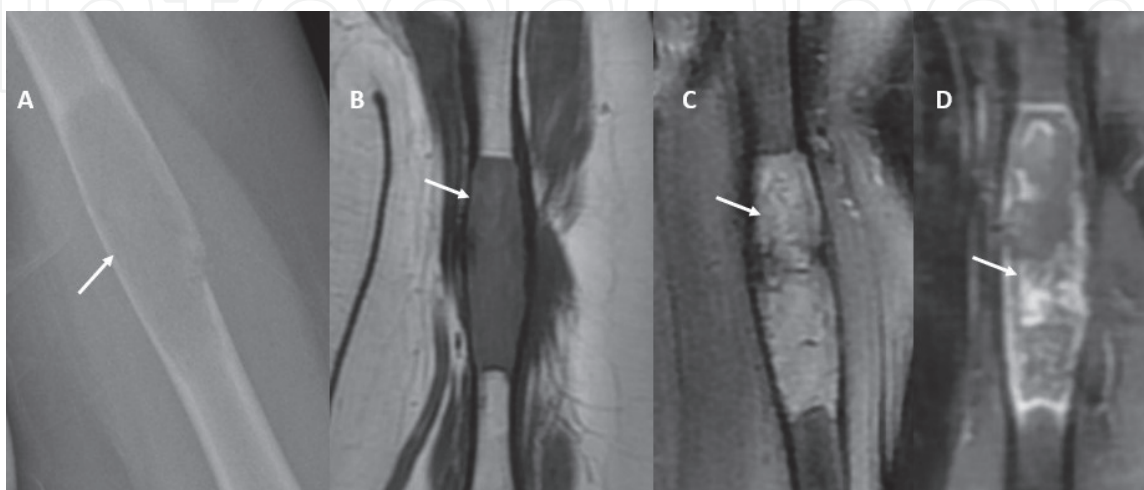


Figure 20. Fibrous dysplasia: Left humerus radiograph (A) demonstrates an expansile diaphyseal lesion (white arrow) with a ground-glass matrix. The lesion (white arrows) demonstrates hypointense T₁ signal (B), heterogeneous but predominantly increased T₂ signal (C), and heterogeneous postcontrast enhancement (D).

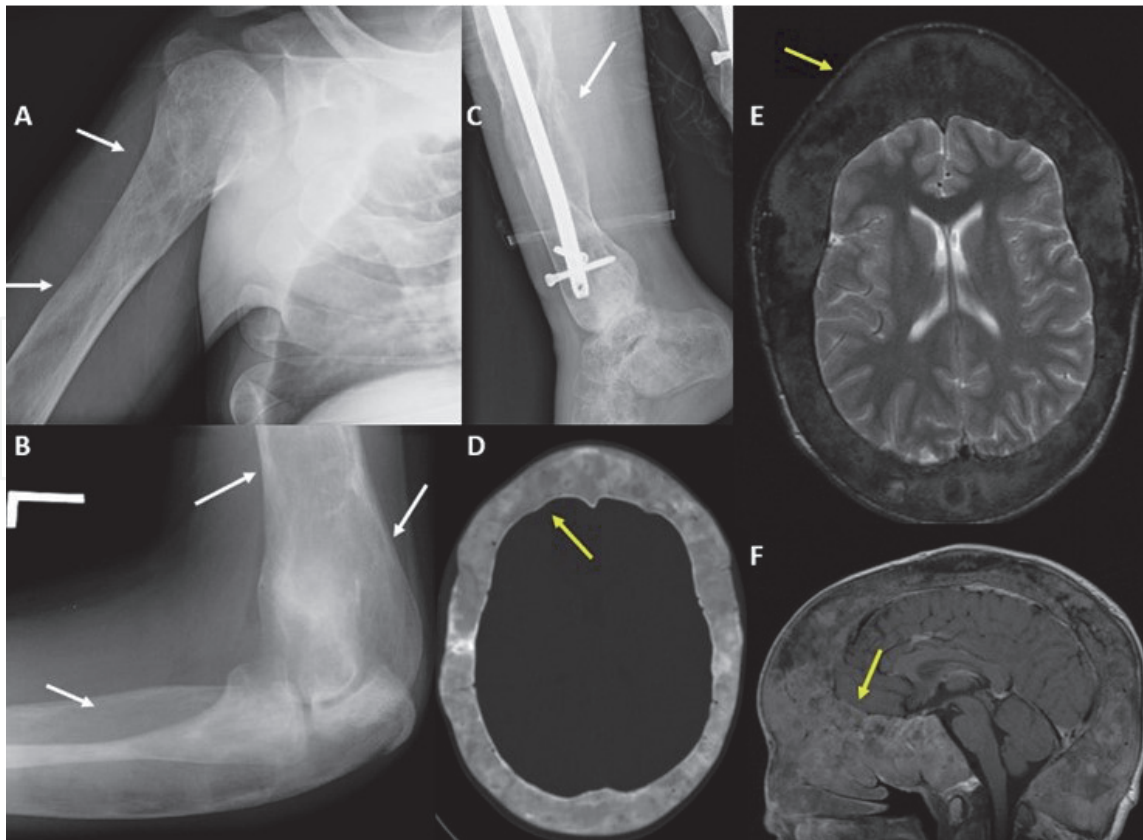


Figure 21. *McCune Albright syndrome: Radiographs (A–C) of the right humerus, left elbow and distal leg demonstrate extensive polyostotic fibrous dysplasia (white arrows) with associated deformities. Axial CT head bone algorithm image (D) demonstrates the characteristic ground-glass appearance of the cranium (yellow arrow) and diffuse widening of diploic space. Axial T2-weighted MR image (E) reveals a heterogenous mixed pattern of low and high SI within the expansile lesion. Also demonstrated is the heterogeneous T1 signal of the thickened calvarium (yellow arrow) in fibrous dysplasia (F).*

mixed lucent-dense pattern between ages of 10–20 years, and some of these lesions may appear ground-glass in adult life. Diagnosing FD lesions purely by MRI is highly challenging because of the highly variable signal demonstrated by these lesions. Typically, the T1 signal is related to the ratio of fibrous tissue to the mineralized matrix, with the FD lesions with high fibrous component showing an intermediate T1 signal, compared to the low signal intensity of lesions with the highly mineralized matrix. The metabolically active fibrous component appears hyperintense on T2-weighted imaging and demonstrates intense enhancement because of high vascularity [68]. Franz et al. described the “milk cloud appearance” of the ground-glass FD lesions on contrast-enhanced T1-weighted MR imaging [69].

Active FD lesions demonstrate increased uptake on ¹⁸F-FDG PET/CT imaging (¹⁸F-NaF is a bone-seeking positron-emitting radiopharmaceutical) which is currently the imaging modality of choice to evaluate FD activity [70].

In most cases, no treatment is required. Curettage and bone grafting is an option if there is a risk for pathologic fracture due to the size of the FD lesion. Persistent moderate-to-severe bone pain of FD can be controlled by intravenous bisphosphonate therapy. However, it should be started only after ensuring the normocalcemic status of the patient and dental evaluation (to decrease the risk of osteonecrosis of the jaw) [71].

3.1 Histiocytic/Langerhans cell lesions

Langerhans cell histiocytosis (LCH)/Eosinophilic granuloma: Langerhans cell histiocytosis is neoplastic proliferation of Langerhans cells/histiocytes in the

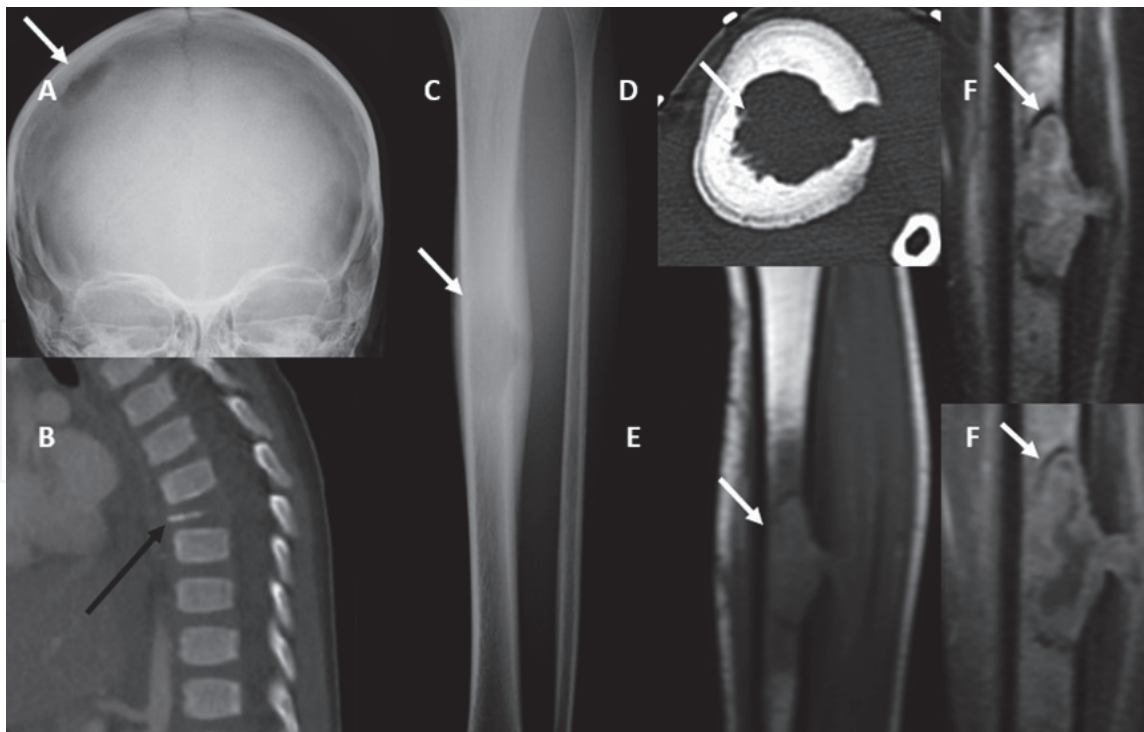


Figure 22.

Eosinophilic granuloma: Skull radiograph (A) demonstrates a punched-out lucent lesion (white arrow) without a mineralized rim. Sagittal bone window image of the thoracic spine (B) reveals a collapsed vertebral body, namely "vertebra plana" (black arrow). Frontal radiograph of left tibia (C) showing an expansile well-defined osteolytic diaphyseal lesion (white arrow) with a benign periosteal reaction. Axial CT bone window image (D) at the level of the diaphyseal lesion demonstrates a punched-out lucent lesion (white arrow). MR images reveal intermediate T1 signal (E), heterogeneous increased T2 signal (F), and thick peripheral enhancement (F).

reticuloendothelial system. These cells produce prostaglandins which are responsible for medullary bone resorption. The incidence of LCH is approximately 1 in 200 000 children [72]. Flat bones are most commonly involved in approximately 65–70% of cases. Skull is the most common site of involvement in flat bones. The monostotic form is more common, seen in approximately 70% of cases [73]. The mean age at diagnosis is typically 5–10 years. Classic radiographic/CT appearance includes solitary or multiple punched-out skull lesions without sclerotic rim (**Figure 22A**). There is a typical beveled edge appearance due to the asymmetrical involvement of inner and outer tables. Spinal lesions may present with vertebra plana (complete collapse and flattening of vertebral body) (**Figure 22B**). When present in long bones, the eosinophilic granuloma is a permeative aggressive appearing lesion with possible associated endosteal scalloping, periosteal reaction, and soft tissue mass (**Figure 22C and D**). The lesion may present in any part of bone but most commonly affects diaphysis. On MRI, these lesions are hypointense on T1, hyperintense on T2/STIR with diffuse post-contrast enhancement (**Figure 22E–G**). Whole-body PET/CT can be utilized to evaluate polyostotic disease and monitor for response to therapy. LCH commonly undergoes spontaneous resolution. If the symptoms persist, excision and curettage are the treatment of choice.

3.2 Giant cell lesions

Giant cell tumor: Giant cell tumor (GCT) of bone, a benign but locally aggressive tumor, comprises multinucleated giant cells interspersed with mononuclear stromal cells. It comprises 20% of all benign bone tumors and 5% of all primary bone tumors. GCT is more prevalent in females and between 20 and 30 years (80%

of cases occur between 20 and 50 years of age). It is rarely seen in the pediatric age group (3% of cases occur before age 14). Though GCT mainly involves long bones, any bone can be affected. The most common location of GCT is around the knee (distal femur and proximal tibia), followed by the distal radius and sacrum [74].

Campanacci and Enneking's clinic radiological staging of GCT: Stage I-The lesion is restricted to the marrow, and bone contour is not affected (cortex may be thinned out); Stage II- Cortical bulging without any signs of rupture; Stage III- Cortical breach with an invasion of soft tissues [75].

Typical radiographic presentation of GCT is that of a circumscribed, eccentric, epiphyseal lytic lesion that extends to the subchondral bone in patients with closed physis. GCT demonstrates a “soap bubble” appearance on radiographs and CT because of bony septae (**Figure 23A and B**). The MR features of GCT are nonspecific. Most commonly, GCT shows hypointense T1 signal and heterogeneous T2 signal (due to collagen content of fibrous components of GCT and deposition of hemosiderin) [76] (**Figure 23C–F**). Contrast administration helps in delineating solid and cystic components. On scintigraphy, there is increased Technetium 99 m-methylene diphosphonate uptake along the periphery of the lesion with central photopenia. An aggressive GCT may demonstrate expansile remodeling, cortical thinning or destruction, a wide zone of transition, and associated soft tissue. Fluid-fluid levels within GCT suggest secondary aneurysmal bone cyst (ABC) formation.

Though intralesional procedures (such as curettage and cement placement) are a preferred approach to treat GCT, they are complicated by recurrence because of residual tumor tissue. He et al. described marginal infiltration as the “paintbrush borders” sign on MRI and advocated it as an independent prognostic factor for local recurrence of GCTB after intralesional curettage [77]. In advanced GCT, Denosumab is recommended for immediate local control and facilitates surgery later [78].

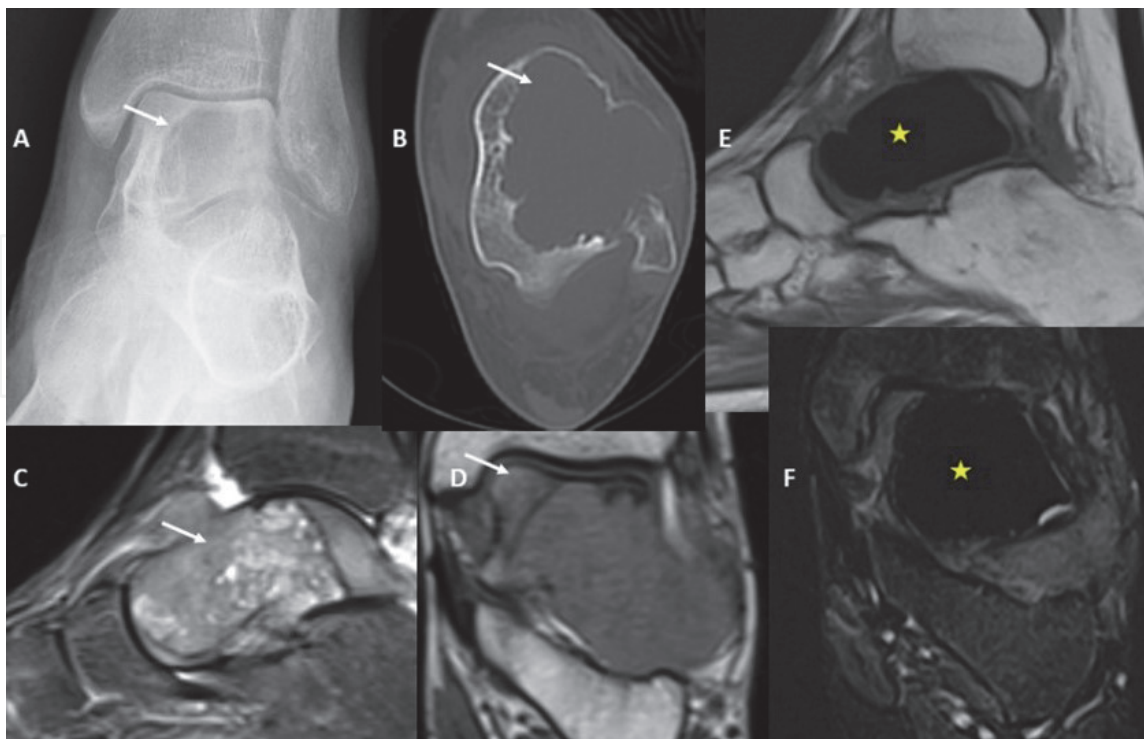


Figure 23.
Giant cell tumor: Frontal radiograph of the left ankle (A) demonstrates a circumscribed lytic lesion (white arrow) in the talus. Axial CT bone window image (B) better depicts the lobulated lytic lesion (white arrow) with scalloped margins. The lytic lesion (white arrow) demonstrates a heterogeneous hyperintense T2 signal (C). On the T1-weighted image (D), the lesion is isointense to muscle. Post-treatment MR images reveal dense hypointense signal on both T1-weighted (E) and T2-weighted (F).

3.3 Vascular lesions

3.3.1 Intraosseous hemangioma

Intraosseous hemangioma (IH) is a benign, slow-growing vascular neoplasm. Though it mainly involves the vertebrae and craniofacial bones, it can rarely involve long bones (mainly intramedullary in metadiaphyseal region; rarely cortical or subperiosteal) [79]. IH are usually identified in females between the age of 30–50 years. The most common pathologic type is cavernous hemangioma. On radiographs, intraosseous hemangiomas may show a “sunburst” or “honeycomb” appearance. On CT, IH may demonstrate the classic “polka dot” sign (due to associated coarse appearance of the trabecular bone), honeycomb appearance of the lytic lesion (because of internal linear trabeculations), or a spiculated “Irish lace” pattern. MRI helps in better delineation of location and extent of the hemangioma. On MRI, IH demonstrates intermediate to high T1 signal, high T2 signal, and diffuse or peripheral enhancement with signal intensity similar to the adjacent vessels [80] (**Figure 24A and B**). Most of the IH lesions are asymptomatic and need no treatment. Symptomatic vertebral hemangiomas without neurologic deficits can be managed by radiotherapy [81].

3.4 Tumor mimickers

1. **Brodie Abscess:** Brodie Abscess is an intraosseous abscess associated with subacute pyogenic osteomyelitis and can often be confused as a bone tumor. There is typically an insidious onset with systemic inflammatory signs, and symptoms are often absent [82]. *Staphylococcus aureus* is the most common organism involved. It typically occurs in the metaphysis of long bones, with proximal and distal tibial metaphyses are most commonly involved. On radiography/CT, Brodie abscess is typically a metaphyseal radiolucent lesion with a sclerotic rim along the long axis of the bone (**Figure 25A**). If a lucent

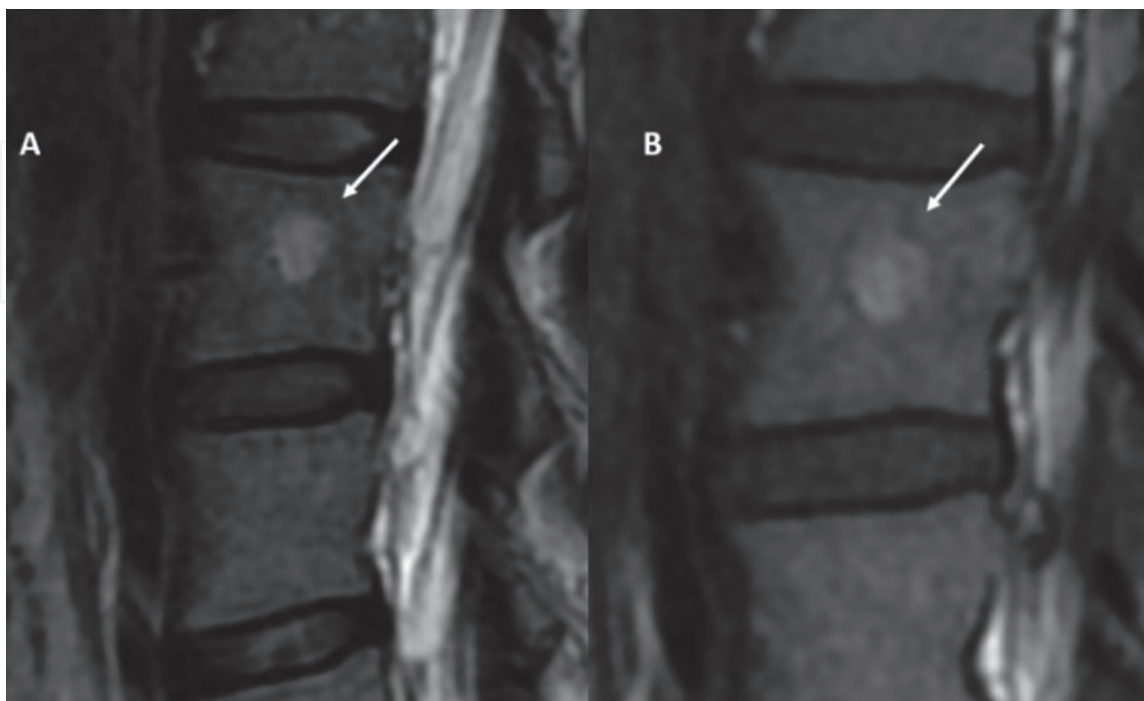


Figure 24. Intraosseous hemangioma: Sagittal MR images of lumbar spine reveal a focal well-circumscribed signal abnormality in the vertebral body (white arrows) that is hyperintense on both T2-weighted (A) and T1-weighted (B) images represent a small vertebral hemangioma.

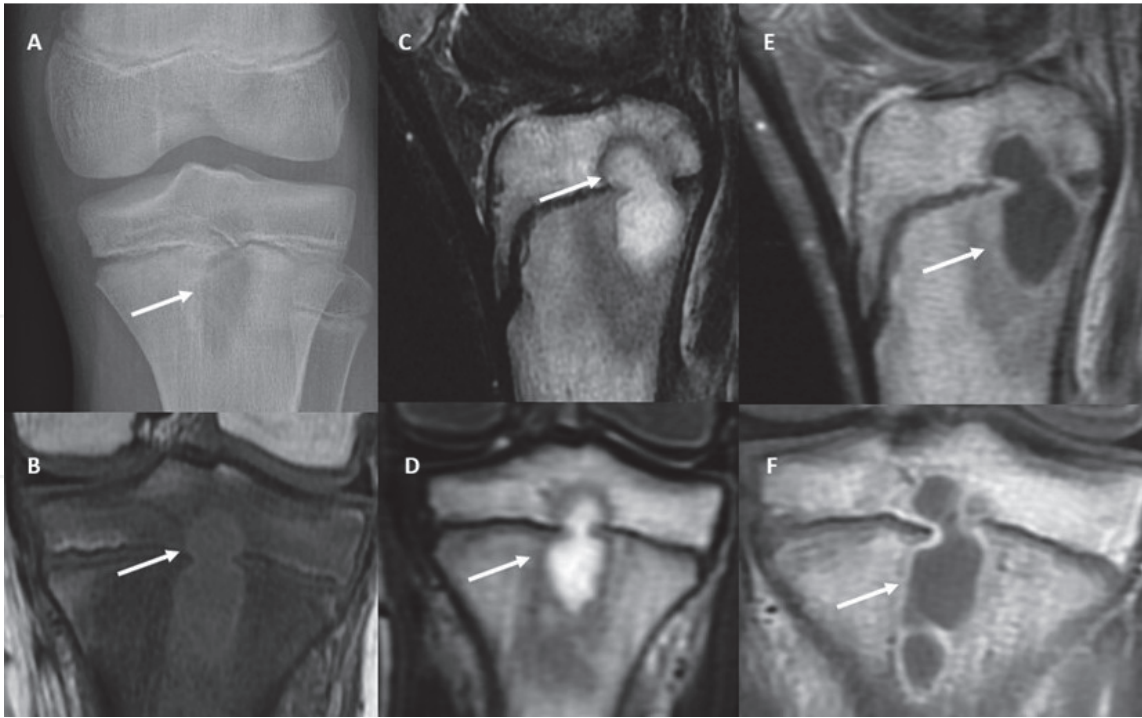


Figure 25. Brodie Abscess: Frontal radiograph of the left knee (A) shows a lucent area (white arrow) with a faintly sclerotic peripheral rim in the proximal tibial epi-metaphyseal region. B demonstrates the "Penumbra sign" with rim lining of the abscess cavity (white arrow) with higher signal intensity than that of the remaining abscess on T1-weighted imaging. The abscess shows increased T2 signal (white arrows; C-D) and peripheral rim enhancement (white arrows) on the postcontrast images (E-F).

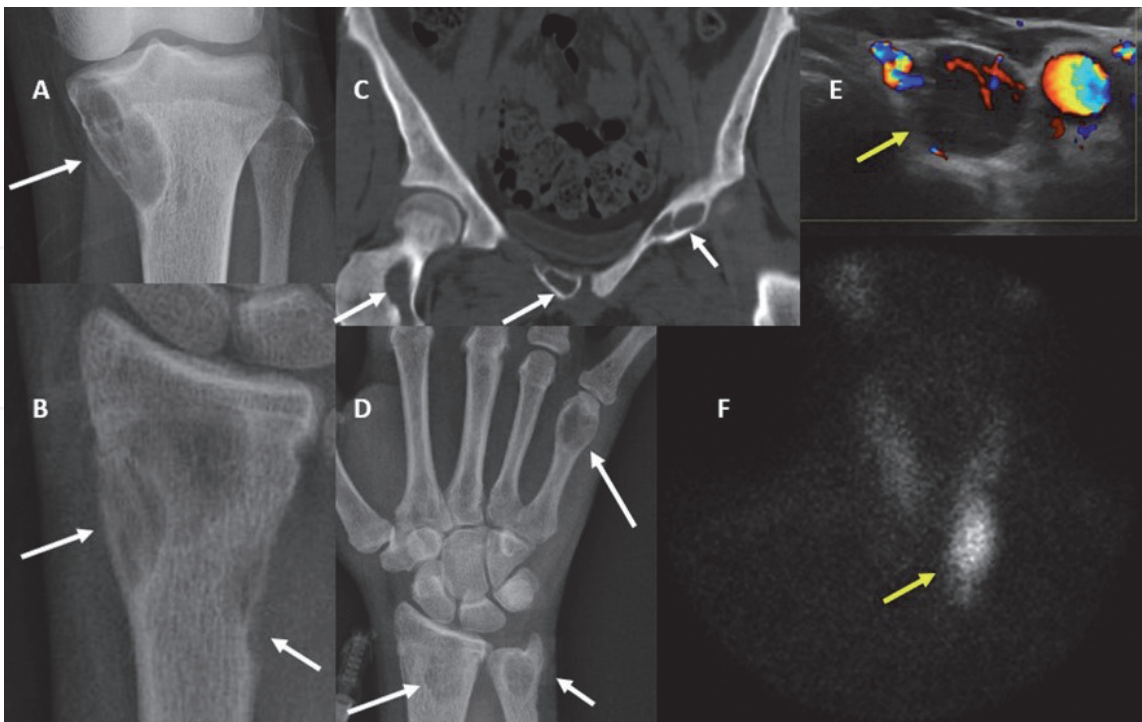


Figure 26. Brown tumor: Frontal radiograph of the left knee (A) shows an eccentric, well-defined, lytic lesion (white arrow) in the proximal tibial epi-metaphyseal region with associated thinning and expansion of cortex. Similar appearing lytic areas (white arrows) are identified in the distal radius (B), pelvic bones and proximal right femur (C), and distal radius and ulna and proximal fifth metacarpal (D). Color flow ultrasound image of the neck (E) demonstrates a well-defined hypochoic solid parathyroid mass (yellow arrow). The parathyroid mass appears as a hot spot (yellow arrow) on nuclear imaging scan (F).

tract extends to physis, diagnosis of Brodie abscess is strongly suggested. There may be associated periosteal reaction. On MRI, there is a T1 hypointense center with T1 hyperintense rim due to peripheral vascularized granulation tissue lining the abscess cavity, which is also termed as “MR penumbra sign” [83] (**Figure 25B–E**). There is typical rim enhancement following contrast administration (**Figure 25F**). Brodie abscess is usually treated with surgical curettage and antibiotic therapy [82].

2. Brown Tumor/Osteitis Fibrosa Cystica: Brown tumor, also known as osteitis fibrosa cystica is the skeletal manifestation of hyperparathyroidism, most commonly related to parathyroid adenoma. Parathormone induces osteoclastic activity, which results in multifocal bone cyst formation and osteopenia. The name brown tumor is derived from color resulting from hemosiderin deposition. Brown tumor is rare, seen in less than 3% of cases of hyperparathyroidism [84]. On radiography/CT, these lesions are typically multifocal well-defined radiolucent lesions with expansion and thinning of the overlying cortex (**Figure 26A–D**). SPECT or planar scintigraphy using Tc-99 m sestamibi shows high radiotracer uptake in parathyroid adenoma (**Figure 26F**). Fusion SPECT–CT can aid in further localization. Brown tumor usually resolves after treatment of hyperparathyroidism in the form of surgical resection of parathyroid adenoma or medical treatment depending on the cause.


IntechOpen

Author details

Jignesh Shah* and Ankita Chauhan
Department of Pediatric Radiology, University of Tennessee Health Science Center,
Memphis, Tennessee, United States

*Address all correspondence to: jshah3@uthsc.edu

IntechOpen

© 2021 The Author(s). Licensee IntechOpen. This chapter is distributed under the terms of the Creative Commons Attribution License (<http://creativecommons.org/licenses/by/3.0>), which permits unrestricted use, distribution, and reproduction in any medium, provided the original work is properly cited. 

References

- [1] S. Noordin, S. Allana, M. Umer, M. Jamil, K. Hilal, and N. Uddin, "Unicameral bone cysts: Current concepts," *Ann Med Surg (Lond)*, vol. 34, pp. 43-49, Oct 2018, doi: 10.1016/j.amsu.2018.06.005.
- [2] E. Mascard, A. Gomez-Brouchet, and K. Lambot, "Bone cysts: Unicameral and aneurysmal bone cyst," *Orthop Traumatol Surg Res*, vol. 101, no. 1 Suppl, pp. S119-S127, Feb 2015, doi: 10.1016/j.otsr.2014.06.031.
- [3] W. F. Jackson, T. N. Theologis, C. L. Gibbons, S. Mathews, and G. Kambouroglou, "Early management of pathological fractures in children," *Injury*, vol. 38, no. 2, pp. 194-200, Feb 2007, doi: 10.1016/j.injury.2006.07.040.
- [4] M. S. Rosario *et al.*, "An unusual case of proximal humeral simple bone cyst in an adult from secondary cystic change," *World J Surg Oncol*, vol. 15, no. 1, p. 102, May 15 2017, doi: 10.1186/s12957-017-1166-8.
- [5] J. N. Shah, H. L. Cohen, A. F. Choudhri, S. Gupta, and S. F. Miller, "Pediatric benign bone tumors: What does the radiologist need to know?: Pediatric imaging," *Radiographics*, vol. 37, no. 3, pp. 1001-1002, May-Jun 2017, doi: 10.1148/rg.2017160143.
- [6] H. Aiba *et al.*, "Treatment of simple bone cysts using endoscopic curettage: A case series analysis," *J Orthop Surg Res*, vol. 13, no. 1, p. 168, Jul 5 2018, doi: 10.1186/s13018-018-0869-z.
- [7] H. Y. Hou, K. Wu, C. T. Wang, S. M. Chang, W. H. Lin, and R. S. Yang, "Treatment of unicameral bone cyst: A comparative study of selected techniques," *J Bone Joint Surg Am*, vol. 92, no. 4, pp. 855-862, Apr 2010, doi: 10.2106/JBJS.I.00607.
- [8] M. G. Weber, J. Fan, and R. Jenkins, "An Uncommon Presentation of an Uncommon Bone Tumor: A Case Study of a Pathologic Fracture of an Intertrochanteric Aneurysmal Bone Cyst," *Cureus*, vol. 11, no. 12, p. e6461, Dec 25 2019, doi: 10.7759/cureus.6461.
- [9] F. Grahneis *et al.*, "Aneurysmal bone cyst: A review of 65 patients," *J Bone Oncol*, vol. 18, p. 100255, Oct 2019, doi: 10.1016/j.jbo.2019.100255.
- [10] R. Capanna, D. A. Campanacci, and M. Manfrini, "Unicameral and aneurysmal bone cysts," *Orthop Clin North Am*, vol. 27, no. 3, pp. 605-14, Jul 1996. [Online]. Available: <https://www.ncbi.nlm.nih.gov/pubmed/8649741>.
- [11] R. J. Sullivan, J. S. Meyer, J. P. Dormans, and R. S. Davidson, "Diagnosing aneurysmal and unicameral bone cysts with magnetic resonance imaging," *Clin Orthop Relat Res*, no. 366, pp. 186-90, Sep 1999, doi: 10.1097/00003086-199909000-00024.
- [12] H. Y. Park *et al.*, "Current management of aneurysmal bone cysts," *Curr Rev Musculoskelet Med*, vol. 9, no. 4, pp. 435-444, Dec 2016, doi: 10.1007/s12178-016-9371-6.
- [13] L. B. Gutierrez, T. M. Link, A. E. Horvai, G. B. Joseph, R. J. O'Donnell, and D. Motamedi, "Secondary aneurysmal bone cysts and associated primary lesions: Imaging features of 49 cases," *Clin Imaging*, vol. 62, pp. 23-32, Jun 2020, doi: 10.1016/j.clinimag.2020.01.022.
- [14] P. P. Lin, C. Brown, A. K. Raymond, M. T. Deavers, and A. W. Yasko, "Aneurysmal bone cysts recur at juxtaphyseal locations in skeletally immature patients," *Clin Orthop Relat Res*, vol. 466, no. 3, pp. 722-728,

Mar 2008, doi: 10.1007/s11999-007-0080-8.

[15] P. Tsagozis and O. Brosjo, "Current Strategies for the Treatment of Aneurysmal Bone Cysts," *Orthop Rev (Pavia)*, vol. 7, no. 4, p. 6182, Dec 28 2015, doi: 10.4081/or.2015.6182.

[16] T. T. Nguyen, J. C. Thelen, and A. A. Bhatt, "Bone up on spinal osseous lesions: A case review series," *Insights Imaging*, vol. 11, no. 1, p. 80, Jun 29 2020, doi: 10.1186/s13244-020-00883-6.

[17] N. A. Avila, A. J. Dwyer, A. Rabel, T. Darling, C. H. Hong, and J. Moss, "CT of sclerotic bone lesions: Imaging features differentiating tuberous sclerosis complex with lymphangiomyomatosis from sporadic lymphangiomyomatosis," *Radiology*, vol. 254, no. 3, pp. 851-857, Mar 2010, doi: 10.1148/radiol.09090227.

[18] A. Ulano *et al.*, "Distinguishing untreated osteoblastic metastases from Enostoses using CT attenuation measurements," *AJR Am J Roentgenol*, vol. 207, no. 2, pp. 362-368, Aug 2016, doi: 10.2214/AJR.15.15559.

[19] S. Bernard, E. Walker, and M. Raghavan, "An approach to the evaluation of incidentally identified bone lesions encountered on imaging studies," *AJR Am J Roentgenol*, vol. 208, no. 5, pp. 960-970, May 2017, doi: 10.2214/AJR.16.17434.

[20] G. P. Nielsen and A. E. Rosenberg, "Update on bone forming tumors of the head and neck," *Head Neck Pathol*, vol. 1, no. 1, pp. 87-93, Sep 2007, doi: 10.1007/s12105-007-0023-4.

[21] L. M. Lehmer, P. Kissel, and B. D. Ragsdale, "Frontal sinus osteoma with osteoblastoma-like histology and associated intracranial pneumatocele," *Head Neck Pathol*, vol. 6, no. 3, pp. 384-388, Sep 2012, doi: 10.1007/s12105-012-0332-0.

[22] A. G. Chiu, I. Schipor, N. A. Cohen, D. W. Kennedy, and J. N. Palmer, "Surgical decisions in the management of frontal sinus osteomas," *Am J Rhinol*, vol. 19, no. 2, pp. 191-7, Mar-Apr 2005. [Online]. Available: <https://www.ncbi.nlm.nih.gov/pubmed/15921220>.

[23] A. Rokade and A. Sama, "Update on management of frontal sinus osteomas," *Curr Opin Otolaryngol Head Neck Surg*, vol. 20, no. 1, pp. 40-44, Feb 2012, doi: 10.1097/MOO.0b013e32834e9037.

[24] M. R. Baruffi, J. B. Volpon, J. B. Neto, and C. Casartelli, "Osteoid osteomas with chromosome alterations involving 22q," *Cancer Genet Cytogenet*, vol. 124, no. 2, pp. 127-31, Jan 15 2001, doi: 10.1016/s0165-4608(00)00327-7.

[25] S. Noordin *et al.*, "Osteoid osteoma: Contemporary management," *Orthop Rev (Pavia)*, vol. 10, no. 3, p. 7496, Sep 5 2018, doi: 10.4081/or.2018.7496.

[26] K. Motamedi and L. L. Seeger, "Benign bone tumors," *Radiol Clin North Am*, vol. 49, no. 6, pp. 1115-34, v, Nov 2011, doi: 10.1016/j.rcl.2011.07.002.

[27] A. Saifuddin, J. White, Z. Sherazi, M. I. Shaikh, C. Natali, and A. O. Ransford, "Osteoid osteoma and osteoblastoma of the spine. Factors associated with the presence of scoliosis," *Spine (Phila Pa 1976)*, vol. 23, no. 1, pp. 47-53, Jan 1 1998, doi: 10.1097/00007632-199801010-00010.

[28] B. C. Carneiro *et al.*, "Osteoid osteoma: the great mimicker," *Insights Imaging*, vol. 12, no. 1, p. 32, Mar 8 2021, doi: 10.1186/s13244-021-00978-8.

[29] J. W. Chai *et al.*, "Radiologic diagnosis of osteoid osteoma: From simple to challenging findings," *Radiographics*, vol. 30, no. 3, pp. 737-749, May 2010, doi: 10.1148/rg.303095120.

- [30] A. Chahal, P. Rajalakshmi, S. A. Khan, S. Rastogi, D. N. Srivastava, and S. Gamanagatti, "CT-guided percutaneous radiofrequency ablation of osteoid osteoma: Our experience in 87 patients," *Indian J Radiol Imaging*, vol. 27, no. 2, pp. 207-215, Apr-Jun 2017, doi: 10.4103/ijri.IJRI_260_16.
- [31] M. A. Galgano, C. R. Goulart, H. Iwenofu, L. S. Chin, W. Lavelle, and E. Mendel, "Osteoblastomas of the spine: A comprehensive review," *Neurosurg Focus*, vol. 41, no. 2, p. E4, Aug 2016, doi: 10.3171/2016.5.FOCUS16122.
- [32] P. K. Avadhanam, S. Vuyyur, and M. K. Panigrahi, "A rare occurrence of osteoblastoma in a child," *J Pediatr Neurosci*, vol. 5, no. 2, pp. 153-156, Jul 2010, doi: 10.4103/1817-1745.76118.
- [33] M. Wu *et al.*, "Diagnostic and management options of Osteoblastoma in the spine," *Med Sci Monit*, vol. 25, pp. 1362-1372, Feb 20 2019, doi: 10.12659/MSM.913666.
- [34] A. Honda *et al.*, "Recurrent lumbar-origin osteoblastoma treated with multiple surgery and carbon ion radiotherapy: A case report," *BMC Musculoskelet Disord*, vol. 21, no. 1, p. 321, May 22 2020, doi: 10.1186/s12891-020-03349-4.
- [35] Z. Huang *et al.*, "Imaging algorithm and multimodality evaluation of spinal osteoblastoma," *BMC Musculoskelet Disord*, vol. 21, no. 1, p. 240, Apr 14 2020, doi: 10.1186/s12891-020-03252-y.
- [36] A. L. Versteeg *et al.*, "Surgical management of spinal osteoblastomas," *J Neurosurg Spine*, vol. 27, no. 3, pp. 321-327, Sep 2017, doi: 10.3171/2017.1.SPINE16788.
- [37] B. D. Elder *et al.*, "Surgical Management of Osteoblastoma of the spine: Case series and review of the literature," *Turk Neurosurg*, vol. 26, no. 4, pp. 601-607, 2016, doi: 10.5137/1019-5149.JTN.14348-15.1.
- [38] C. T. Kraft, R. J. Morrison, and H. A. Arts, "Malignant transformation of a high-grade osteoblastoma of the petrous apex with subcutaneous metastasis," *Ear Nose Throat J*, vol. 95, no. 6, pp. 230-3, Jun 2016. [Online]. Available: <https://www.ncbi.nlm.nih.gov/pubmed/27304442>.
- [39] M. J. Walden, M. D. Murphey, and J. A. Vidal, "Incidental enchondromas of the knee," *AJR Am J Roentgenol*, vol. 190, no. 6, pp. 1611-1615, Jun 2008, doi: 10.2214/AJR.07.2796.
- [40] T. Reisler, S. L. Viviano, and M. Granick, "Osseous tumor of the hand: finger enchondroma," *Eplasty*, vol. 15, p. ic4, 2015. [Online]. Available: <https://www.ncbi.nlm.nih.gov/pubmed/25671055>.
- [41] S. Capkin, A. Cavit, K. Yilmaz, and T. Kaleli, "Surgical Treatment of Solitary Enchondromas of the Hand," *Cureus*, vol. 12, no. 4, p. e7497, Apr 1 2020, doi: 10.7759/cureus.7497.
- [42] T. De Coninck *et al.*, "Dynamic contrast-enhanced MR imaging for differentiation between enchondroma and chondrosarcoma," *Eur Radiol*, vol. 23, no. 11, pp. 3140-3152, Nov 2013, doi: 10.1007/s00330-013-2913-z.
- [43] C. Silve and H. Juppner, "Ollier disease," *Orphanet J Rare Dis*, vol. 1, p. 37, Sep 22 2006, doi: 10.1186/1750-1172-1-37.
- [44] T. C. Pansuriya, H. M. Kroon, and J. V. Bovee, "Enchondromatosis: insights on the different subtypes," *Int J Clin Exp Pathol*, vol. 3, no. 6, pp. 557-69, Jun 26 2010. [Online]. Available: <https://www.ncbi.nlm.nih.gov/pubmed/20661403>.
- [45] J. Yang, W. Tian, X. Zhu, and J. Wang, "Chondroblastoma in the long

bone diaphysis: A report of two cases with literature review,” *Chin J Cancer*, vol. 31, no. 5, pp. 257-264, May 2012, doi: 10.5732/cjc.011.10402.

[46] S. J. Swarts, J. R. Neff, S. L. Johansson, M. Nelson, and J. A. Bridge, “Significance of abnormalities of chromosomes 5 and 8 in chondroblastoma,” *Clin Orthop Relat Res*, no. 349, pp. 189-93, Apr 1998, doi: 10.1097/00003086-199804000-00023.

[47] W. Chen and L. M. DiFrancesco, “Chondroblastoma: An Update,” *Arch Pathol Lab Med*, vol. 141, no. 6, pp. 867-871, Jun 2017, doi: 10.5858/arpa.2016-0281-RS.

[48] P. T. Weatherall, G. E. Maale, D. B. Mendelsohn, C. S. Sherry, W. E. Erdman, and H. R. Pascoe, “Chondroblastoma: Classic and confusing appearance at MR imaging,” *Radiology*, vol. 190, no. 2, pp. 467-474, Feb 1994, doi: 10.1148/radiology.190.2.8284401.

[49] S. Cappelle, S. Pans, and R. Sciote, “Imaging features of chondromyxoid fibroma: Report of 15 cases and literature review,” *Br J Radiol*, vol. 89, no. 1064, p. 20160088, Aug 2016, doi: 10.1259/bjr.20160088.

[50] H. S. Kim *et al.*, “MRI of chondromyxoid fibroma,” *Acta Radiol*, vol. 52, no. 8, pp. 875-80, Oct 1 2011, doi: 10.1258/ar.2011.110180.

[51] J. S. Bhamra *et al.*, “Chondromyxoid fibroma management: A single institution experience of 22 cases,” *World J Surg Oncol*, vol. 12, p. 283, Sep 12 2014, doi: 10.1186/1477-7819-12-283.

[52] K. Tepelenis *et al.*, “Osteochondromas: An updated review of epidemiology, pathogenesis, clinical presentation, radiological features and treatment options,” *In Vivo*, vol. 35, no. 2, pp. 681-691, Mar-Apr 2021, doi: 10.21873/invivo.12308.

[53] A. M. de Souza and R. Z. Bispo Junior, “Osteochondroma: ignore or investigate?,” *Rev Bras Ortop*, vol. 49, no. 6, pp. 555-64, Nov-Dec 2014, doi: 10.1016/j.rboe.2013.10.002.

[54] M. D. Murphey, J. J. Choi, M. J. Kransdorf, D. J. Flemming, and F. H. Gannon, “Imaging of osteochondroma: Variants and complications with radiologic-pathologic correlation,” *Radiographics*, vol. 20, no. 5, pp. 1407-1434, Sep-Oct 2000, doi: 10.1148/radiographics.20.5.g00se171407.

[55] J. V. Bovee, “Multiple osteochondromas,” *Orphanet J Rare Dis*, vol. 3, p. 3, Feb 13 2008, doi: 10.1186/1750-1172-3-3.

[56] C. M. Czajka and M. R. DiCaprio, “What is the proportion of patients with multiple hereditary exostoses who undergo malignant degeneration?,” *Clin Orthop Relat Res*, vol. 473, no. 7, pp. 2355-2361, Jul 2015, doi: 10.1007/s11999-015-4134-z.

[57] A. J. Degnan and V. M. Ho-Fung, “More than epiphyseal Osteochondromas: Updated understanding of imaging findings in dysplasia Epiphysealis Hemimelica (Trevor disease),” *AJR Am J Roentgenol*, vol. 211, no. 4, pp. 910-919, Oct 2018, doi: 10.2214/AJR.18.19712.

[58] L. A. Semenova and I. V. Bulycheva, “[Chondromas (enchondroma, periosteal chondroma, enchondromatosis)],” *Arkh Patol*, vol. 69, no. 5, pp. 45-8, Sep-Oct 2007. [Online]. Available: <https://www.ncbi.nlm.nih.gov/pubmed/18074822>.

[59] P. Robinson *et al.*, “Periosteal chondroid tumors: Radiologic evaluation with pathologic correlation,” *AJR Am J Roentgenol*, vol. 177, no. 5, pp. 1183-1188, Nov 2001, doi: 10.2214/ajr.177.5.1771183.

- [60] M. Blaz, P. Palczewski, J. Swiatkowski, and M. Golebiowski, "Cortical fibrous defects and non-ossifying fibromas in children and young adults: The analysis of radiological features in 28 cases and a review of literature," *Pol J Radiol*, vol. 76, no. 4, pp. 32-9, Oct 2011. [Online]. Available: <https://www.ncbi.nlm.nih.gov/pubmed/22802852>.
- [61] G. S. Goodin, B. L. Shulkin, R. A. Kaufman, and M. B. McCarville, "PET/CT characterization of fibrous defects in children: 18F-FDG uptake can mimic metastatic disease," *AJR Am J Roentgenol*, vol. 187, no. 4, pp. 1124-1128, Oct 2006, doi: 10.2214/AJR.06.0171.
- [62] L. M. Bowers, D. M. Cohen, I. Bhattacharyya, J. C. Pettigrew, Jr., and M. F. Stavropoulos, "The non-ossifying fibroma: A case report and review of the literature," *Head Neck Pathol*, vol. 7, no. 2, pp. 203-210, Jun 2013, doi: 10.1007/s12105-012-0399-7.
- [63] K. Jamshidi, P. Motaghi, A. Bagherifard, M. Eigi, H. H. Al-Baseese, and A. Mirzaei, "Comparison of Characteristic Features and Local Recurrence in Syndromic Versus Non-syndromic Multifocal Non-ossifying Fibroma," *J Orthop Sci*, Aug 17 2020, doi: 10.1016/j.jos.2020.06.010.
- [64] A. R. Kinnunen, R. Sironen, and P. Sipola, "Magnetic resonance imaging characteristics in patients with histopathologically proven fibrous dysplasia-a systematic review," *Skeletal Radiol*, vol. 49, no. 6, pp. 837-845, Jun 2020, doi: 10.1007/s00256-020-03388-x.
- [65] E. Gokce and M. Beyhan, "Radiological imaging findings of craniofacial fibrous dysplasia," *Turk Neurosurg*, vol. 30, no. 6, pp. 799-807, 2020, doi: 10.5137/1019-5149.JTN.24627-18.2.
- [66] M. Wilson and C. Snyderman, "Fibro-osseous lesions of the Skull Base in the pediatric population," *J Neurol Surg B Skull Base*, vol. 79, no. 1, pp. 31-36, Feb 2018, doi: 10.1055/s-0037-1617440.
- [67] M. K. Javaid *et al.*, "Best practice management guidelines for fibrous dysplasia/McCune-Albright syndrome: A consensus statement from the FD/MAS international consortium," *Orphanet J Rare Dis*, vol. 14, no. 1, p. 139, Jun 13 2019, doi: 10.1186/s13023-019-1102-9.
- [68] A. Butt, K. Patel, K. Agrawal, A. Arya, and J. Singh, "Fibrous dysplasia of the clivus - a case study and literature review," *Radiol Case Rep*, vol. 16, no. 2, pp. 230-236, Feb 2021, doi: 10.1016/j.radcr.2020.11.019.
- [69] D. Franz *et al.*, "Milk cloud appearance-a characteristic sign of fibrous dysplasia on contrast-enhanced MR imaging," *Eur Radiol*, vol. 29, no. 7, pp. 3424-3430, Jul 2019, doi: 10.1007/s00330-019-06245-1.
- [70] G. Z. Papadakis *et al.*, "(18) F-NaF PET/CT IMAGING IN FIBROUS DYSPLASIA OF BONE," *J Bone Miner Res*, vol. 34, no. 9, pp. 1619-1631, Sep 2019, doi: 10.1002/jbmr.3738.
- [71] R. Chapurlat and M. A. Legrand, "Bisphosphonates for the treatment of fibrous dysplasia of bone," *Bone*, vol. 143, p. 115784, Feb 2021, doi: 10.1016/j.bone.2020.115784.
- [72] H. Park, M. Nishino, J. L. Hornick, and E. D. Jacobsen, "Imaging of Histiocytosis in the era of genomic medicine," *Radiographics*, vol. 39, no. 1, pp. 95-114, Jan-Feb 2019, doi: 10.1148/rg.2019180054.
- [73] J. Zaveri, Q. La, G. Yarmish, and J. Neuman, "More than just Langerhans cell histiocytosis: A radiologic review of histiocytic disorders," *Radiographics*,

vol. 34, no. 7, pp. 2008-2024, Nov-Dec 2014, doi: 10.1148/rg.347130132.

[74] C. J. Chakarun, D. M. Forrester, C. J. Gottsegen, D. B. Patel, E. A. White, and G. R. Matcuk, Jr., "Giant cell tumor of bone: Review, mimics, and new developments in treatment," *Radiographics*, vol. 33, no. 1, pp. 197-211, Jan-Feb 2013, doi: 10.1148/rg.331125089.

[75] H. M. Pereira, E. Marchiori, and A. Severo, "Magnetic resonance imaging aspects of giant-cell tumours of bone," *J Med Imaging Radiat Oncol*, vol. 58, no. 6, pp. 674-678, Dec 2014, doi: 10.1111/1754-9485.12249.

[76] L. S. Shi, Y. Q. Li, W. J. Wu, Z. K. Zhang, F. Gao, and M. Latif, "Imaging appearance of giant cell tumour of the spine above the sacrum," *Br J Radiol*, vol. 88, no. 1051, p. 20140566, Jul 2015, doi: 10.1259/bjr.20140566.

[77] Y. He *et al.*, "Magnetic resonance feature of "paintbrush borders" sign as a novel way to predict recurrence of giant cell tumor of bone after curettage: A pilot study," *J Int Med Res*, vol. 46, no. 2, pp. 710-722, Feb 2018, doi: 10.1177/0300060517720345.

[78] L. van der Heijden *et al.*, "The clinical approach toward giant cell tumor of bone," *Oncologist*, vol. 19, no. 5, pp. 550-61, May 2014, doi: 10.1634/theoncologist.2013-0432.

[79] A. Rigopoulou and A. Saifuddin, "Intraosseous hemangioma of the appendicular skeleton: Imaging features of 15 cases, and a review of the literature," *Skeletal Radiol*, vol. 41, no. 12, pp. 1525-1536, Dec 2012, doi: 10.1007/s00256-012-1444-z.

[80] Q. Zhou, L. Lu, Z. Yang, S. Su, and G. Hong, "Hemangioma of long tubular bone: Imaging characteristics with emphasis on magnetic resonance imaging," *Skeletal Radiol*, vol. 49, no.

12, pp. 2029-2038, Dec 2020, doi: 10.1007/s00256-020-03527-4.

[81] K. Yao, F. Tang, L. Min, Y. Zhou, and C. Tu, "Multifocal intraosseous hemangioma: A case report," *Medicine (Baltimore)*, vol. 98, no. 2, p. e14001, Jan 2019, doi: 10.1097/MD.00000000000014001.

[82] N. van der Naald, D. P. J. Smeeing, R. M. Houwert, F. Hietbrink, G. A. M. Govaert, and D. van der Velde, "Brodie's abscess: A systematic review of reported cases," *J Bone Jt Infect*, vol. 4, no. 1, pp. 33-39, 2019, doi: 10.7150/jbji.31843.

[83] A. Afshar and A. Mohammadi, "The "penumbra sign" on magnetic resonance images of Brodie's abscess: A case report," *Iran J Radiol*, vol. 8, no. 4, pp. 245-248, Dec 2011, doi: 10.5812/iranradiol.4493.

[84] C. Xie, M. Tsakok, N. Taylor, and K. Partington, "Imaging of brown tumours: A pictorial review," *Insights Imaging*, vol. 10, no. 1, p. 75, Jul 29 2019, doi: 10.1186/s13244-019-0757-z.